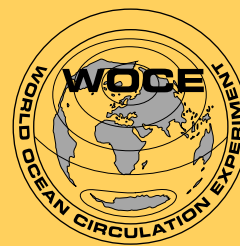


International

WOCE

Newsletter



Number 19

June 1995

IN THIS ISSUE

		page
<input type="checkbox"/> News from the IPO		
<i>The Way Forward</i>	W.J. Gould	2
<input type="checkbox"/> Science: Pacific		
<i>The Deep Western Boundary Current at 17°S in the Pacific Ocean</i>	H. Banks et al.	3
<i>Subarctic Gyre of the Western Pacific</i>	B. Taft	6
<i>Volume and Heat Transport, Tasman Sea, May-June '93 (PR11/PR13)</i>	S. Chiswell and B. Stanton	8
<i>A Hydrography in the Southern Philippine Sea: From WOCE Hydrographic Programme Section PR15 and PR24</i>	T. Kawano et al.	11
<i>WOCE P19 in the Eastern South Pacific</i>	L. Talley and M. Tsuchiya	14
<i>Overview of WOCE Field Work in the Pacific Ocean</i>	N.P. Holliday	18
<input type="checkbox"/> Science: Atlantic and others		
<i>Intense Mixing of Antarctic Bottom Water in the Equatorial Atlantic</i>	K. Polzin et al.	20
<i>One-time Section A23 Completed on RRS James Clark Ross Cruise 10</i>	K. Heywood and B. King	24
<i>WHP Section A3 Across 36°N Aboard RV Professor Multanovskiy</i>	V. Tereschenkov et al.	25
<i>Modelling Radiocarbon Uptake by the Southern Ocean</i>	J. Ribbe and M. Tomczak	27
<i>Neutral Density</i>	D. Jackett and T. McDougall	30
<input type="checkbox"/> Data Issues		
<i>New Depth Equation for 'Old' Sparton XBT-7 Expendable Bathythermographs</i>	P. Rual et al.	33
<i>Locating WOCE Data on the Internet</i>	N.P. Holliday	35
<i>Rapid Dissemination of WOCE Science Results</i>	P.M. Saunders	36
<input type="checkbox"/> Other Programmes		
<i>The Global Ocean Observing System (GOOS)</i>	N. Flemming	37
<input type="checkbox"/> Meetings		
<i>The Second WMO International Symposium on Assimilation of Observations in Meteorology and Oceanography</i>	R. Tokmakian	38
<i>Meeting Timetable</i>		40

The Way Forward

W. John Gould, Director, WOCE IPO

Extended life for WOCE

Well its now official – WOCE as an international component of WCRP has been extended to 2002. At the meeting of the WCRP Joint Scientific Committee (JSC) in Pasadena in April, Breck Owens (WOCE SSG Co-Chair) presented a summary of WOCE achievements, and the strategy WOCE plans to adopt for its later phase. This phase will be one of Analysis, Interpretation, Modelling and Synthesis (AIMS) and will extend beyond the end of WOCE observations in 1997 to 2002.

The document “Status, Achievements and Prospects for WOCE (1995)” that backed up the presentation has just been published by the WOCE IPO and will be widely circulated. The IPO also plans to produce copies of the transparencies used in our presentation to the JSC and to distribute them to National Committees for them to use to highlight WOCE achievements within their country. The JSC congratulated WOCE on its forward-looking approach and achievements and on its having evolved its scientific oversight mechanisms into those appropriate for the AIMS phase.

A major challenge

While the “Status” document outlines in general terms, the strategy to be adopted, a major challenge remains in defining the means, both scientific and logistical, by which WOCE can both produce basin-wide and global syntheses of the numerous and diverse data sets and develop the appropriate assimilation schemes for bringing WOCE data and models together.

This will be a task for the new WOCE Synthesis and Modelling WG (SMWG) under its co-chairs Andrew Bennett and Lynne Talley. The SMWG membership is now complete and the first meeting is being planned. Its work will also require a close partnership with the WOCE Data Products Committee whose task it will be to ensure the timely delivery of the required data sets.

Resources required for WOCE research beyond 1997 will be less than for the observational period but will still be substantial. At the meeting of the Intergovernmental WOCE Panel in Paris in early June, national representatives will be presented with the need for these long-term resources for maintenance of the WOCE data systems and for the manpower and computer resources. Above all there is a fundamental need for the rapid availability of WOCE data sets.

New measurements

The WOCE field programme continues. The Indian Ocean survey will have completed 6 sections or parts (I3, 4, 5E, 5W, 7C, 8N, 9N) by June 1995. Clearance to work

in Indian waters was received just in time to allow work to be carried out. The moored array ICM1 has been deployed in the Agulhas Current and will be recovered in 1996. In the South Atlantic/Southern Ocean section A23 from the Weddell Sea to Brazil was completed as were sections A13 and 14. Was A23 the first cruise to have its own home page on the World Wide Web with data products and photographs available with the ship still at sea?

Another notable event was the launch on 21 April of ERS-2. It is still in its commissioning phase but so far all systems except the scatterometer seem to be working well. It will run in tandem with ERS-1 for a 3–9 month period after which ERS-1 will be put into standby mode.

TOGA Conference

The Tropical Ocean Global Atmosphere (TOGA) experiment, a WCRP programme like WOCE, formally ended in 1994. To mark this, a TOGA Conference was held in April in Melbourne, Australia. I can tell you that Melbourne is a very “user friendly” city and our local hosts did an excellent job. The meeting was a stimulating affair of morning plenary lectures and afternoon posters highlighting TOGA science results and attended by over 350 delegates. Central themes were the substantial progress that has been made in prediction of ENSO events (this has come from the close association of modellers and observationalists) and a growing understanding of the global impacts of ENSO. The surprising persistence of Pacific thermal anomalies in the 1990s has proved that there is still plenty of scope for refinement of the models.

WOCE too is planning a major conference in mid-1998 and I hope to be able to give you more details of this and of forthcoming WOCE science workshops in the next Newsletter. The TOGA conference ended in a “TOGA” party in the Old Melbourne Gaol. I hope by now all the Melbourne hotels have got their sheets back. What would be an appropriate venue for a WOCE party and what should we wear? Ideas to the IPO please.

Footnote

We still do not have a firm date for the WOCE IPO move to Southampton but the new building is now almost complete and looks very impressive with such ships as the QE2 berthed nearby. We hope to be able to entertain visitors there from October onwards and will be publicising our new address, phone and fax numbers in the next Newsletter.

Thanks to all of you who are taking the time to send us articles. Our revised mailing list includes many new readers and shows that there’s lots of interest in what WOCE is doing.

The Deep Western Boundary Current at 17°S in the Pacific Ocean

Helene Banks, Southampton University Department of Oceanography, Southampton, UK; John Bullister, Pacific Marine Environmental Laboratory, Seattle, USA.; Sheldon Bacon and Harry Bryden, James Rennell Centre for Ocean Circulation, Southampton, UK

The transpacific WOCE Hydrographic Programme section P21 aboard RV Melville crossed the deep western boundary current over the Tonga Trench at a latitude of 17.5°S in June 1994 (Fig. 1). As in previous crossings of the boundary current, there is a broad slope to the deep isotherms, isohalines and isopycnals below 3000 dbar extending about 1000 km eastward from the Tonga-Kermadec Ridge to 160°W (Figs. 2a and 2b) that represents the signature of the northward flowing bottom water (Warren, 1981). Here we estimate the transport of the deep western boundary current, compare it with transports at other latitudes, and show that the northward flowing water has a measurable chlorofluorocarbon signal in its deeper portions.

The deep flow close to the Ridge and over the Trench has the slight salinity maximum and silica minimum (Fig. 2c) at about 4000 dbar that characterises the Atlantic water element of the Lower Circumpolar Deep Water (LCDW). Below this Atlantic influence, salinity decreases and silica increases as the bottom waters of Antarctic origin become dominant. It is in this region of Antarctic influence that we observe the maximum CFC signal at about 5000 dbar (Fig. 3).

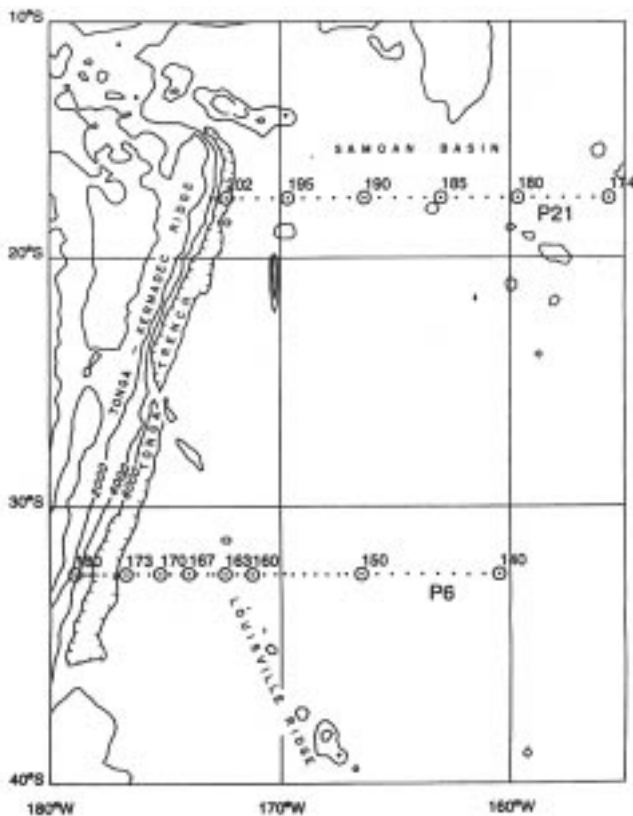


Figure 1. Location map.

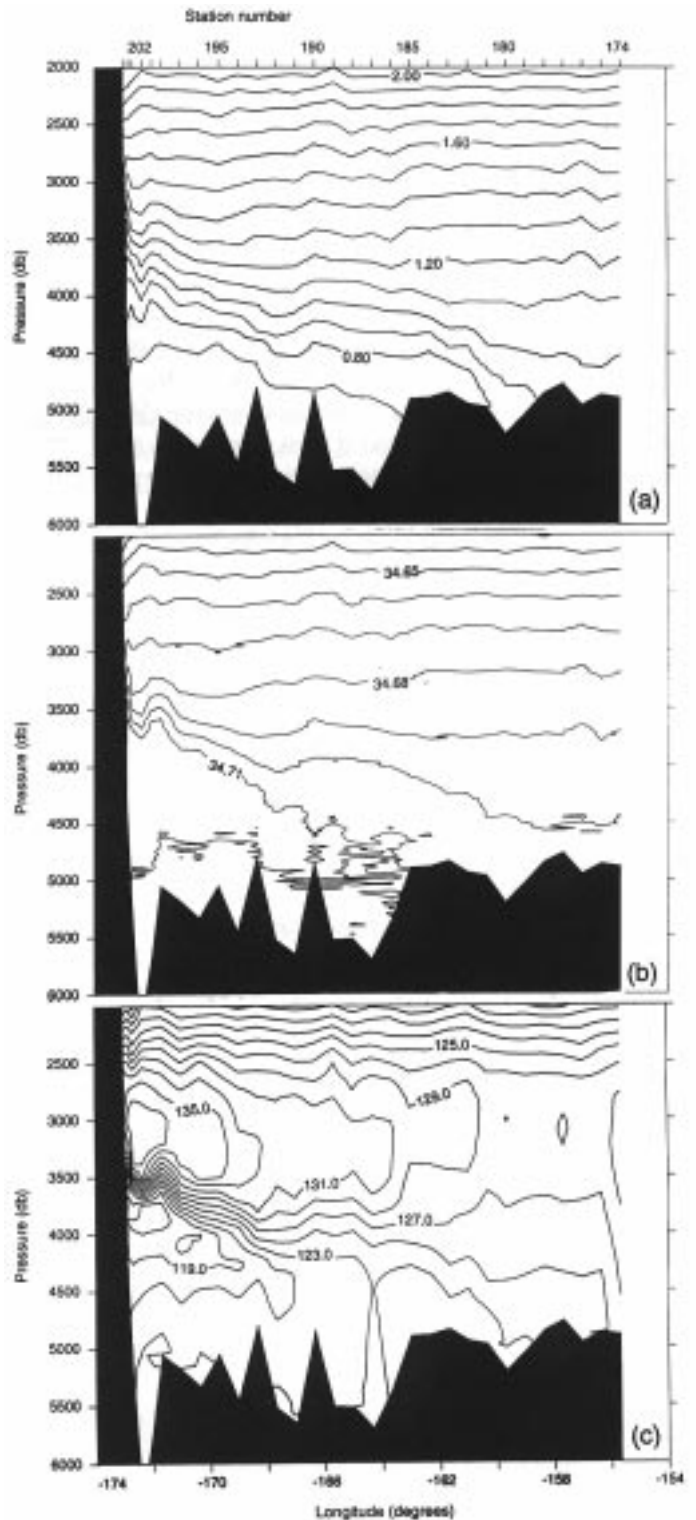


Figure 2. (a) Potential Temperature (°C), (b) Salinity (psu), (c) Silica ($\mu\text{mol/l}$) at 17.5°S.

Above the northward flowing deep western boundary current, there is a silica maximum centred at 3200 dbar against the eastern flank of the Ridge. It is a maximum both in vertical and zonal directions and the high silica suggests that this is southward flowing Pacific Deep Water (PDW), perhaps a southward flowing deep western boundary current of the most populous water mass in the world oceans (Worthington, 1981).

Because of the juxtaposition of northward flowing LCDW beneath southward flowing PDW against the boundary, we choose a reference level for geostrophic calculations of transport between the northward and southward flowing cores at 1.2°C potential temperature surface. Such a reference level is conveniently the same as has been used in other boundary current analyses (Johnson and Toole, 1993; Wijffels, 1993; Johnson *et al.*, 1994).

The northward transport of waters colder than 1.2°C is quite uniform and broad. Except for a small reversal (at station pair 190-191) and a recirculation over the eastern edge of the Tonga Trench (station pair 199-202), the northward transport steadily accumulates for 1300 km out to station 180 and achieves a final value of 13.6 Sv. The transport-weighted potential temperature of this northward flow of LCDW across 17.5°S is 0.762°C.

The southward flow above the 1.2°C isotherm appears more concentrated against the boundary. Integrating the velocities upward to 2200 dbar, there is a relatively uniform southward flow that accumulates to a transport of -5.1 Sv station at 195, roughly 330 km from the Ridge, with only a single reversal at station pair 199-202. There is broad northward flow further to the east so that the net southward transport integrated out to station 180 is only -1.9 Sv. Hence, some of the southward boundary flow of PDW may be recirculating back into the Samoan Basin.

Now we will look at a similar transpacific section at a latitude of 32.5°S; WOCE section P6 aboard RV Knorr which crossed the deep western boundary current in June 1992. We can see similar features in the isotherms, isohalines

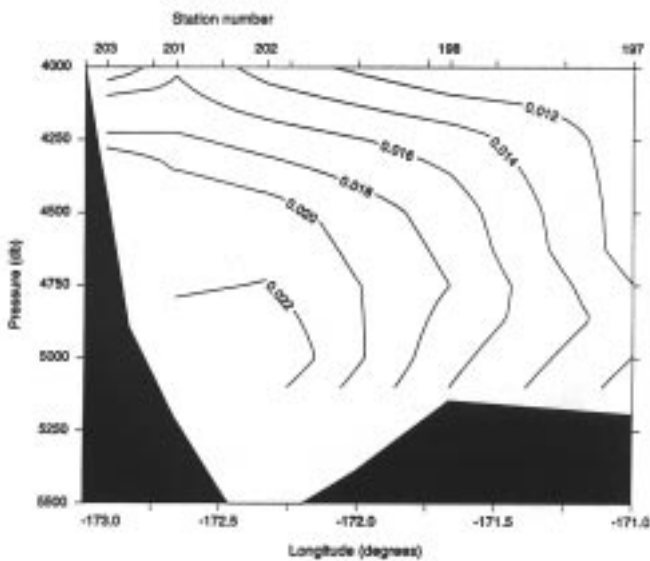


Figure 3. CFC-11 (pM kg^{-1}) at 17.5°S

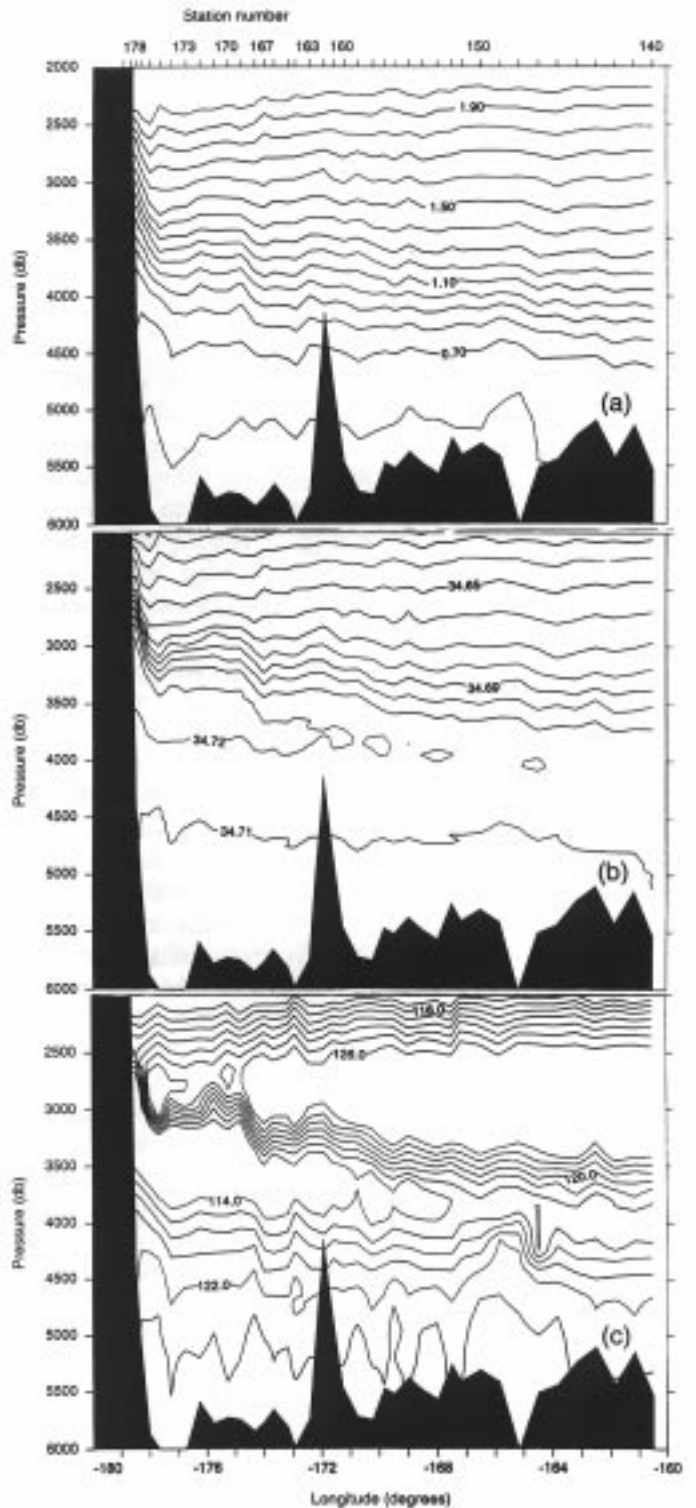


Figure 4: (a) Potential Temperature ($^{\circ}\text{C}$), (b) Salinity (psu), (c) Silica ($\mu\text{mol/l}$) at 32.5°S.

and isopycnals extending for almost 2000 km from the ridge to 160°W (Figs. 4a and 4b). However, at this latitude the salinity maximum and silica minimum (Fig. 4c) indicating Atlantic influence in the LCDW are now higher in the water column, at about 3500 dbar; and the silica maximum indicating the core of PDW is now centred at 2800 dbar. Thus the Atlantic core of northward flowing LCDW deepens by 500 dbar following the flow and the core of southward flow shallows by 400 dbar following the

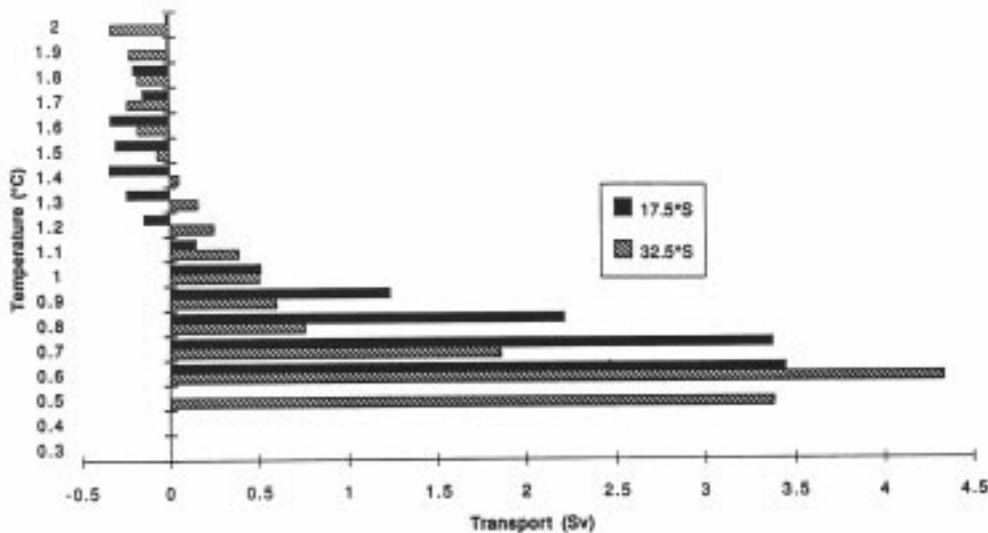


Figure 5. Transport (Sv) in 0.1°C temperature classes. 17.5°S is denoted bold, 32.5°S is denoted shaded.

flow. As before, we set the reference level by the juxtaposition between the properties of LCDW of southern origin in the deeper waters and the properties of PDW of northern origin to choose the 1.5°C potential temperature surface as level of no motion at 32.5°S .

In waters colder than 1.5°C the northward flow is predominant although not quite as uniform as previously. We observe reversals at station pairs 163–164, 166–167 and 169–170 and, again, there appears to be a recirculation over the eastern edge of the trench (172–173). We choose to define the eastern edge of the boundary current by the first ridge in the bathymetry (Louisville ridge), giving an accumulated transport of 14.7 Sv at station 162, 650 km from the ridge.

Above the 1.5°C isotherm we have integrated the velocities upward to 2200 dbar. The southward flow is concentrated next to the ridge; out to station 175 (115 km from the ridge) where the transport accumulates to -2.86 Sv. This is substantially less than the -5.1 Sv of southward flow we found at 17.5°S indicating that some of the southward flowing PDW at 17.5°S may be recirculating. At station 162 the net transport of PDW is only -1.72 Sv, again suggesting that some horizontal recirculation is taking place away from the boundary region.

Fig. 5 shows the transport at 17.5°S and 32.5°S in 0.1°C temperature classes. The northward transport at 32.5°S in the temperature classes 1.2°C to 1.5°C is 0.45 Sv. Hence we estimate that 14.2 Sv flows northward, as waters colder than 1.2°C in the deep western boundary current at 32.5°S and such transport is effectively the same as the 13.6 Sv found at 17.5°S . Further north, Wijffels (1993) estimates the net transport of LCDW to be 12.1 Sv across 14°S and 9.6 Sv across 10°N . By 24.5°N , Bryden *et al.* (1991) estimate the northward transport of LCDW is 4.9 Sv and it is confined to waters with temperature less than 1.06°C .

At 32.5°S the transport-weighted potential temperature of the northward flow colder than 1.2°C is 0.696°C which

would imply that the northward flowing deep western boundary current has increased by 0.066°C in temperature by the time it reaches 17.5°S . For the southward flow we find that the transport-weighted potential temperature, above the 1.5°C isotherm, at 17.5°S is 1.687°C while at 32.5°S it is 1.856°C – an increase in temperature of 0.169°C as the PDW flows southward.

These results suggest that as the water masses flow away from their source in the western boundary current, significant vertical and lateral mixing takes place leading to net temperature increases. The recirculation

which we observe in both the northward and southward flow may be indicative of recirculation gyres like those observed in the North Atlantic (Schmitz and McCartney, 1993). The presence of recirculating flows in all of the deep boundary currents that we have examined suggests that a countercurrent is common to all western boundary currents and it is reminiscent of the Munk (1950) model solutions for western boundary currents based on lateral viscosity arguments. We hope that further work on these deep boundary currents will give us insight into the nature of the mixing and how to quantify it.

References

- Bryden, H.L., D.H. Roemmich, and J.A. Church, 1991: Ocean heat transport across 24°N in the Pacific. *Deep-Sea Res.*, 38(3), 297–324.
- Johnson, G.C., D.L. Rudnick, and B.A. Taft, 1994: Bottom water variability in the Samoa Passage. *J. Mar. Res.*, 52(2), 177–196.
- Johnson, G.C., and J.M. Toole, 1993: Flow of deep and bottom waters in the Pacific at 10°N . *Deep-Sea Res.*, 40(2), 371–394.
- Munk, W.H., 1950: On the wind-driven ocean circulation. *J. Meteor.*, 7(2), 79–93.
- Schmitz, W.J., and M.S. McCartney, 1993: On the North Atlantic Circulation. *Rev. Geophys.*, 31(1), 29–49.
- Warren, B.A., 1981: Deep circulation of the World Ocean. In: *Evolution of physical oceanography - Scientific surveys in honor of Henry Stommel*, B.A. Warren and C. Wunsch, Eds., MIT Press, 623pp.
- Wijffels, S.E., 1993: Exchanges between hemispheres and gyres: A direct approach to the mean circulation of the Equatorial Pacific. Ph.D. Thesis. MIT/WHOI, WHOI-93-42.
- Worthington, L.V., 1981: The water masses of the World Ocean: Some results of a fine-scale census. In: *Evolution of physical oceanography - Scientific surveys in honor of Henry Stommel*, B.A. Warren and C. Wunsch, Eds., MIT Press, 623pp.

Subarctic Gyre of the Western Pacific

Bruce Taft, Pacific Marine Environmental Laboratory/NOAA, 7600 Sand Point Way NE, Seattle, WA 98115, USA

The cyclonic subarctic gyre of the Pacific is bounded on the west by the southwest-flowing East Kamchatka Current (EKC) and the southern limb of the gyre is the eastward-flowing Subarctic Current. In August 1992 a deep section was made on the John Vickers starting at the 200 m isobath off Kamchatka and ending up south of the Kuroshio (Fig. 1). It crosses the Kurile-Kamchatka Trench (>6 km), the two eastern branches of the Shatsky Rise and two deep bowls (>6000 m) north and east of the Shatsky Rise. This section constitutes the northern portion of the WOCE one-time survey line P13. Thirty-mile station spacing was maintained to 36°N; station intervals increased to 40 miles south of 36°N.

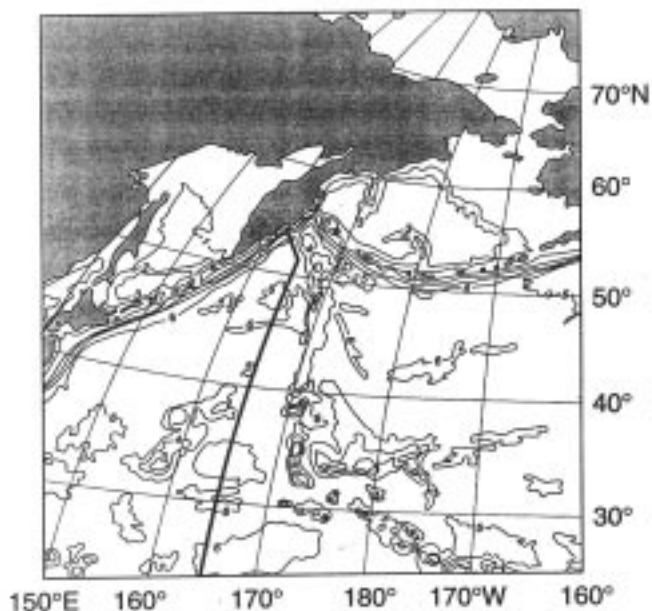


Figure 1. Location of CTD stations on the northern portion of WOCE section P13. Bathymetry is from Plate 1 of Craig *et al.* (1981); depths are in km.

The shallow temperature section (Fig. 2) shows the characteristic features of the subarctic in the summer.

- (1) The coldest surface temperature (and lowest salinities) are found at the three inshore stations off Kamchatka.
- (2) Temperature at the near-surface temperature minimum is less than 1°C at the Kamchatka boundary which is indicative of the Bering Sea origin of this water. Although the minimum is continuous to 46°N, there are two distinct pools of colder water in the minimum separated by a band of warmer water. The southern cold region (<2°C) is water that has been transported southward along the Kurile Island to about 45°N

where most of the water in the EKC turns eastward to form the Subarctic Current (Favorite *et al.*, 1976). The EKC receives an admixture of very cold Okhotsk Sea temperature minimum water which is entrained into the boundary current at the Bussol' Strait (46°N) (PICES Working Group 1, 1995) and then transported eastward.

- (3) Underneath the temperature minimum is a temperature maximum with values greater than 3.5°C at the boundary; a lateral minimum in this feature occurs in the latitude range of the Subarctic Current. This minimum can be traced in the Subarctic Current across the entire subarctic Pacific (Favorite *et al.*, 1976).
- (4) There is a sharp temperature/salinity front at 100 m at 46°N which marks the southern boundary of the Subarctic Current; since both salinity and temperature increase to the south, there is not a corresponding density front.
- (5) South of this current boundary there is a transition region with a mixture of subtropical and subarctic water such that subarctic features persist (temperature minimum and halocline) but they have been modified by mixing processes (temperature at the minimum increases to >3.75° and the strength of the halocline is strongly reduced).
- (6) The Subarctic Front marks the southern boundary of water with subarctic characteristics and the disappearance of the subarctic halocline. At the surface it is marked at 42°N by a 4°C drop in temperature and it extends to about 700 m. Using the traditional definition of the Front (Favorite *et al.*, 1976) to be the location of the 34 isohaline, the deeper portion would be near 40°N rather than 42°N. This definition would suggest that the near-surface expression of the Front on this section is displaced 200 km to the north of the Front at depth. The frontal structure shown on this section is not commonly observed.
- (7) The north boundary of the Kuroshio is at 35°N.

The baroclinic shear of the EKC is indicated on the temperature section by deepening of the isotherms toward the boundary; this tendency is traceable to 3100 m. It is associated with freshening of the water nearest to the boundary so that the temperature and salinity distributions act in concert to increase the horizontal density gradient and baroclinic current. Note that there is a 300 km warm-core structure offshore from the EKC. In this discussion it will be referred to as an anticyclonic eddy.

The silicate distribution (Fig. 3) shows a continuous maximum in the vertical at about 2000 m with highest values in excess of 190 µmol/kg in the EKC. High silicate

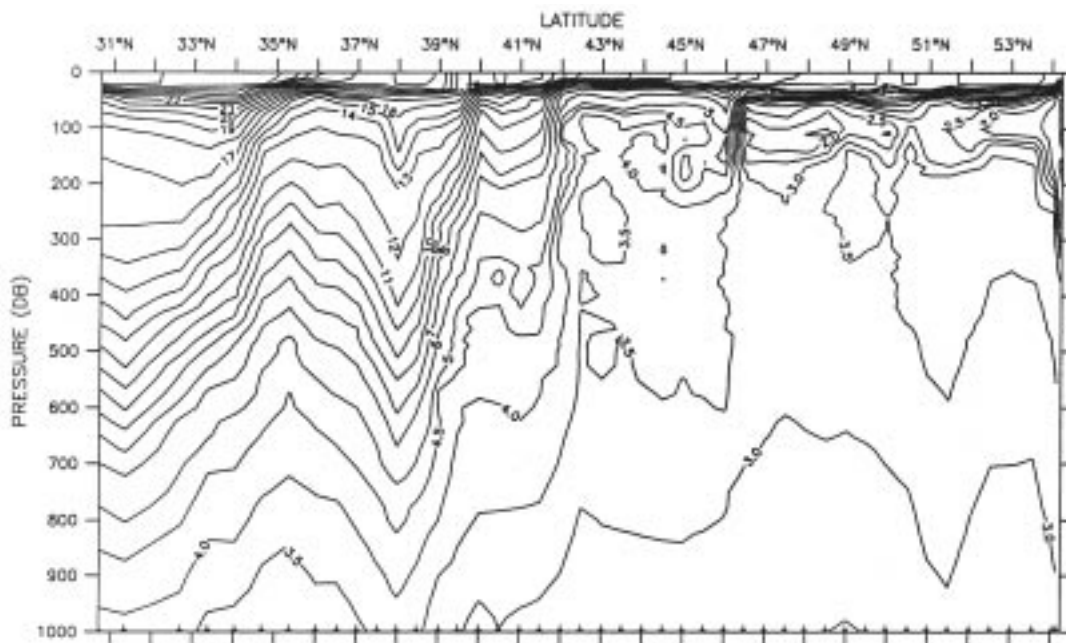


Figure 2. Distribution of potential temperature ($^{\circ}\text{C}$) in upper 1 km along the northern portion of P13.

at the boundary, in the EKC, extends to 3700 m; below 4000 m silicate at the boundary is low relative to the interior, consistent with transport from the south, where lower abyssal values occur. The source of the high silicate in the EKC is southward flow out of the silicate-rich western basin of the Bering Sea through the Kamchatka Strait (Reed *et al.*, 1993). Near-bottom values of silicate in the Bering Sea are uniformly higher than the N. Pacific values. The eastern Aleutian Basin of the Bering Sea contains the highest silicate values in the world ocean ($>225 \mu\text{mol/kg}$) (Reed *et al.*, 1993). Based on the silicate distribution, it is reasonable to choose a surface of 3700 db to compute geostrophic transport of the EKC because it appears to be a surface separating southward transport (above) and northward transport (below). This surface also will be used to calculate the transport across the section north of the Subarctic Front.

There are three major features that have significant transports: EKC; deep anticyclonic eddy adjacent to the EKC (51.5°N); and the Subarctic Current. The boundaries and volume transports of these three elements can be determined by plotting the cumulative transport (relative to 3700 db).

	Boundaries	Transport ($10^6 \text{ m}^3/\text{s}$)
East Kamchatka Current	$53.5^{\circ}\text{--}54.25^{\circ}\text{N}$	17
Anticyclonic eddy	51.5°N (centre)	3 (net)
Subarctic Current	$45^{\circ}\text{--}9^{\circ}\text{N}$	18

The transport of the Subarctic Current is not sensitive to the choice of a deeper reference surface – the eastward transport increases only $0.3 \times 10^6 \text{ m}^3/\text{s}$ if the transport is calculated relative to the bottom. The cumulative transport between the Subarctic Front and Kamchatka is zero and the southwestward transport of the EKC and the eastward transport of the Subarctic Current are not significantly

different. This agreement supports the idea that the Subarctic Current is formed from water that has been transported southward in the EKC and then separates from the boundary to flow eastward. The presence of the strong, deep, large-scale anticyclonic feature, presumed to be an eddy, may have affected the structure and transport of the EKC. The scale of this feature is considerably larger than the anticyclonic eddies near Kamchatka reported by Solomon and Ahnläs (1978) from an analysis of satellite images of the surface temperature patterns.

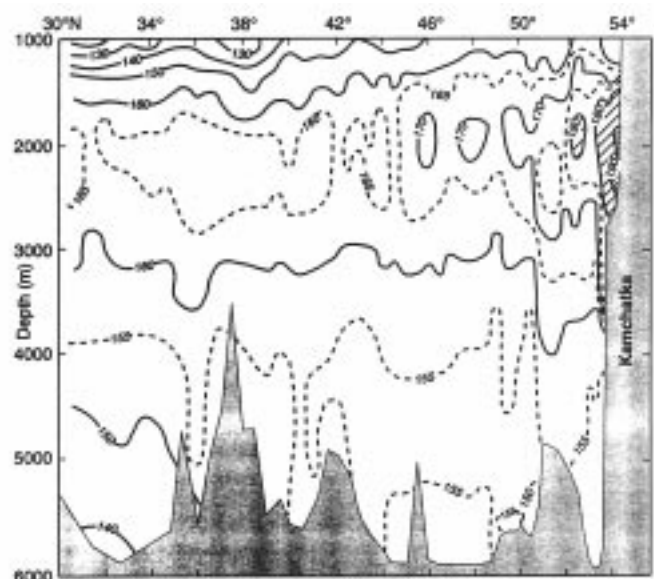


Figure 3. Distribution of silicate ($\mu\text{mol/kg}$) below 1 km along the northern portion of P13.

References

- Craig, H., W.S. Broecker, and D. Spencer, 1981: GEOSECS Pacific Expedition, Vol. 4, Sections and Profiles, 1973–1974. Nat. Science Foundation, Washington, DC, 251pp.
- Favorite, F., A.J. Dodimead, and K. Nasu, 1976: Oceanography of the Subarctic Pacific region. Bull. Int. North Pacific Comm., 33, 1–187.
- PICES Working Group 1, 1995: Physics of the Okhotsk Sea and Oyashio Region, Chapter II.5, in press.
- Reed, R., G.V. Khen, P.J. Stabeno, and A.V. Verkhunov, 1993: Water properties and flow over the deep Bering Sea basin, summer 1991. Deep-Sea Res., 40, 2325–2334.
- Solomon, H., and K. Ahnläs, 1978: Eddies in the Kamchatka Current. Deep-Sea Res., 25, 403–410.

Volume and Heat Transports, Tasman Sea, May–June 1993 (PR13N, PR11)

Stephen Chiswell and Basil Stanton, New Zealand Oceanographic Institute, National Institute for Water and Atmospheric Research, PO Box 14-901, Kilbirnie, Wellington

WOCE repeat hydrography lines PR13N and PR11 cross the Tasman Sea along 43°15'S and 30°05'S (Fig. 1). These lines are important because they span the East Australian Current, and occupying them allows measurements to be made of the mass and heat fluxes in this little-observed current. Since 1989 these lines have been occupied 6 and 5 times, respectively, by Australian, New Zealand and United States institutes. The New Zealand contribution to the repeat hydrography took place in May–June 1993, when both PR11 and PR13N were occupied by the New Zealand Oceanographic Institute (NZOI) using the RV Akademik Lavrentyev under charter from the Russian Academy of Sciences. This note presents the data collected during that cruise, along with estimates of the heat and volume fluxes from calculations of the geostrophic and Ekman transports.

Fig. 1 shows the cruise track. As well as the northern and southern legs, the Tasman Sea was closed off with an approximately north-south section made between New Zealand and the eastern end of the northern section.

The Tasman Sea bathymetry is complicated by the presence of the Lord Howe Rise, the Norfolk Ridge, and Three Kings Ridge. Below 2000 m the Tasman Sea is separated into three distinct basins: the Tasman Basin, the New Caledonia Trough, and the Norfolk Basin. Closest to Australia, the Tasman Basin is closed to the north, but in the south opens to the deep South Indian Basin. The New Caledonia Trough is open to the north, whereas the Norfolk Basin is essentially enclosed.

CTD casts were made to within 10 m of the bottom along the cruise track according to WOCE spacing requirements, except that delays due to bad weather caused us to increase the station spacing along the southern section. Along PR11, stations were made in the same positions as on the WOCE one-time section P6 in 1992.

Geostrophic velocities normal to the sections were calculated using the thermal wind equation. We chose the level of no motion to be 2000 dbar, principally to be consistent with previous calculations (e.g., Ridgway and Godfrey, 1994), and because the maximum depth seen in the eastern section was close to 2000 m, but there is other

evidence to suggest that this may be a reasonable choice. Warren (1973) used the same level for the area east of New Zealand, arguing that it lies above the deep tracer features (which are indicative of meridional flow) and in the middle of the deep oxygen-minimum layer which he suggests is a region of slow horizontal velocity (although in the Tasman Sea, the oxygen minimum tends to be slightly shallower than 2000 dbar).

Ekman transports were calculated for each leg by integrating the Ekman transport along the ship track using the wind stress calculated from the mean wind over the duration of the cruise. Winds were obtained from European Centre for Medium-range Weather Forecasting (ECMWF) products at 2.5° grid spacing.

Surface temperature along PR13N shows values of 12°C near New Zealand increasing to 14°C near Australia, with surface salinity increasing from about 34.8 to 35.5 (Figs. 2a and 2b). These properties are indicative of subtropical water (STW), and show that the subtropical

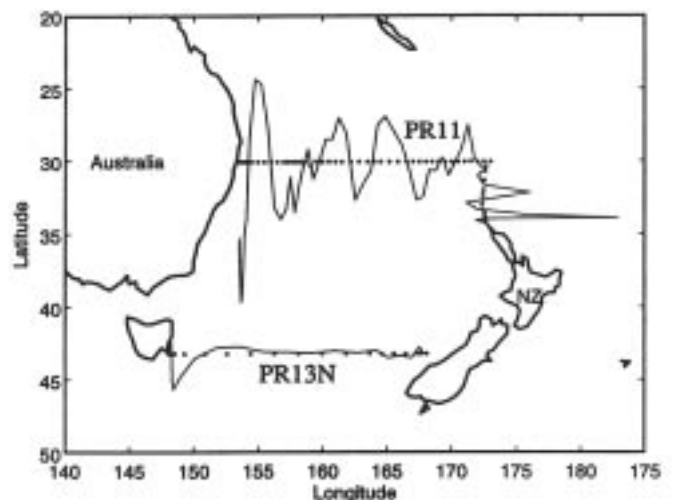


Figure 1. Map showing station locations (o) and surface geostrophic currents for three sections taken in May 1993. Surface currents are scaled so that 10° of latitude corresponds to a speed of 1 m s⁻¹.

convergence during this period was south of 43°15'S. Near New Zealand, salinity has a weak subsurface maximum of about 35.0, but near Australia, maximum salinities occur at the surface.

PR13N passes entirely over the Tasman Basin, and the deepest water depths in this survey occur along this section. Coolest potential temperatures of about 0.6°C are found at 4500 m, close against the Tasmanian slope. Isotherms in this region (*e.g.*, $\theta = 0.8$) slope down to the east, which would indicate a deep western boundary current to the north, but this temperature gradient is to some extent compensated by salinity, which increases to the east. Between the Tasmanian slope and about 160°E potential density isopycnals slope down to the east, but then slope upwards until they meet the New Zealand slope, indicating northward flow on the west side of the Tasman Basin and southward flow on the east side. Since the Tasman Basin is closed to the north, this reflects cyclonic circulation of the bottom water within the basin, with deep bottom water entering the basin on the west, and returning slightly warmer and saltier to the east. Warren (1973), in an analysis of the SCORPIO section along 43°S, noted warming of the bottom water in the Tasman Sea was more likely to be due to downwards diffusion of heat rather than geothermal warming – and estimated bottom speeds of $6 \cdot 10^{-2} \text{ cm s}^{-1}$ (*i.e.*, very weak). In a similar manner, the increase in

salinity is likely to be a result of downwards diffusion of salt. The circulation of bottom water represents a net flux of salt and heat out of the Tasman Sea.

Along the northern leg, PR11, surface temperatures are about 18–19°C near New Zealand, increasing to about 22°C in the East Australian Current. Uplifts in temperature and salinity isopleths indicate the presence of two cold-core (cyclonic) eddies centred near 156°E and 167°E, with a weaker eddy centred near 163°E.

The highest salinities in the deep water in this section (S~34.725) are lower than the highest seen in the southern section (S~34.73), this is consistent with the diffusive attenuation of the deep salinity maximum as it moves downstream, but we note that Warren (1973) saw higher salinities downstream in the salinity maximum, and suggested that the deep water may be heterogeneous.

The eastern section, taken to close off the Tasman Sea was made along the Three Kings Ridge, and has maximum depths of about 2000 m. The sections show a gradual cooling and freshening of surface waters going south.

Above 2000 dbar, the southern section shows a band of southward flow adjacent to Tasmania with currents as strong as 0.23 m s^{-1} (Fig. 3). Elsewhere currents were considerably weaker, with flows mostly less than 0.05 m s^{-1} . Deep flows, below 2000 dbar, show slow northward (inflow) along the Tasmanian slope, with slow outflow along the New Zealand slope.

Along the northern section, currents were considerably stronger. Adjacent to the Australian coast, flows associated with an inshore branch of the East Australian Current were as strong as 1.0 m s^{-1} southward. The eddies seen in the temperature and salinity sections are clearly seen in the geostrophic current, with northward flow on their west side, and southward flow on the east side. Strongest northward flow at the surface is about 0.5 m s^{-1} . As with the southern section, the deep circulation shows northward flow along the Tasmanian slope returning southwards along the New Zealand slope, although the magnitudes of this abyssal circulation are higher in the northern section. Banded geostrophic currents along the eastern section reflect the slopes seen in the isotherms. There is strong westward flow up to 0.4 m s^{-1} just north of New Zealand. Table 1 presents basin-wide integrated volume, heat, and salt transports. The geostrophic volume transport into the Tasman Sea along 30°5'S was 11.9 Sv ($1 \text{ Sv} = 10^6 \text{ m}^3 \text{ s}^{-1}$), the transport out through the southern and eastern sections were 6.6 and 6.7 Sv, respectively, leading to a net

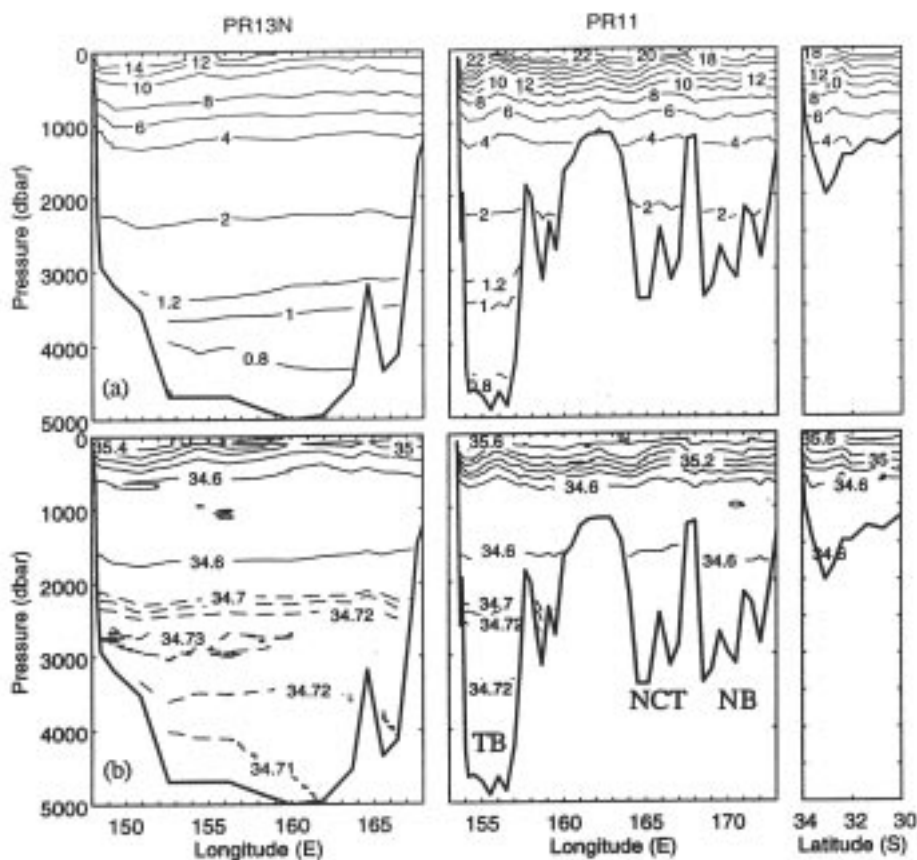


Figure 2. Vertical distribution of potential temperature (a) and salinity (b) from the three sections. Above 2000 dbar the contours are spaced every 2°C and 0.2 PSU, below 2000 dbar they are every 0.2°C and 0.01 PSU. TB: Tasman Basin, NCT: New Caledonia Trough, NB: Norfolk Basin.

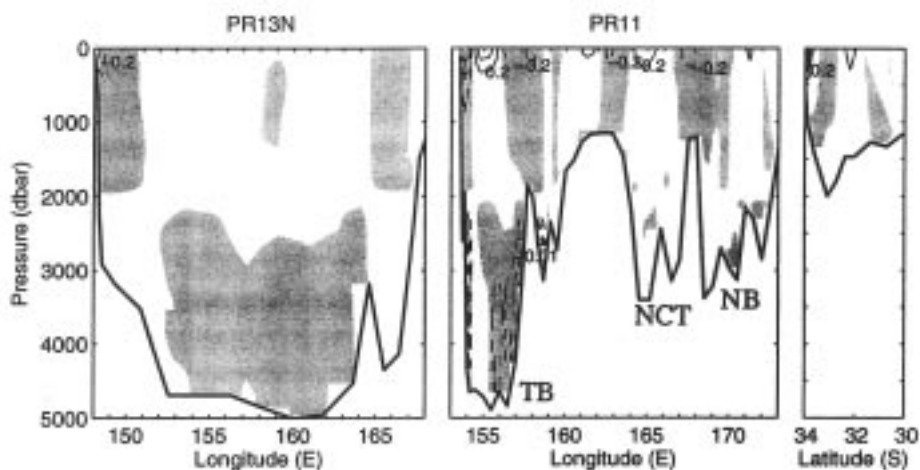


Figure 3. Normal geostrophic current from the three sections, computed with a level of no motion at 2000 dbar. Southward or westward flowing current is shaded. Contours are spaced every 0.2 m s^{-1} , below 2000 dbar contours are spaced every 0.01 m s^{-1} .

outflow of approximately 1.4 Sv. To some extent this is balanced by a total Ekman transport into the Tasman Sea of 0.5 Sv, mostly along the southern section (0.36 Sv), leaving a total volume deficit of 0.9 Sv.

Integrating the heat fluxes into the Tasman Sea indicates a net heat inflow of $1.2 \cdot 10^{14} \text{ W s}^{-1}$ into the sea. To balance this exactly by heat flow out into the atmosphere, would require an average heat flux of approximately 48 W m^{-2} over the entire sea. Our calculations show a near balance in salt. An inflow of $4.3 \cdot 10^8 \text{ kg s}^{-1}$ entering through the northern section is approximately evenly split into salt advected through the southern and eastern boundaries.

In principle, the geostrophic flow in the Tasman Sea should balance the wind-driven Ekman flow. The volume imbalance we attain of 0.8 Sv could have been closed by using a different level of no motion, so by itself, does not give any indication of how robust our calculations are, but the close balance of both volume and salt transports increases our confidence in the integrated heat flows.

Figs. 1 and 3 suggest that the East Australian Current is characterised by a strong eddy field and this appears to be typical of the current (*e.g.*, Boland and Church, 1981). The circulation within the gyre is apparently largely unstructured, with a high degree of eddy activity, making it impossible to define an eastern boundary to the current. Previous estimates of the transport in the East Australian Current vary widely, from 12 to 45 Sv (Hamon, 1965; Wyrtki, 1962), but in part this variability may be due to lack of consistency in defining the limits of the flow.

Our volume transport between Australia and New Zealand is more than recently determined by Bailey *et al.* (1993). They obtained a mean flow of 7.1 Sv, with a 2.6 Sv standard deviation for six realisations of an XBT section

from Brisbane to Fiji. Part of this difference is because they used a reference level of 800 m, but using this level in our case still leads to a transport of 9.8 Sv. Ridgway and Godfrey (1994) using a large set of expendable bathythermograph data show an annual-mean net transport of 9.4 Sv across the Tasman Sea at 28°S , compared to our value of 11.9 Sv at $30^\circ 5'\text{S}$. At 43°S , they obtain an annual mean transport of 6 Sv, about the same as we get.

Our value of the net heat loss to the atmosphere (48 W m^{-2}) is comparable to annual-mean value of 54 W m^{-2} quoted by Ridgway and Godfrey (1994) for a slightly large region encompassing the Tasman Sea (from 43°S to 28°S).

Acknowledgements

We would like to thank M. Grieg, M. Herzfeld, J. Iseli, W. Main, B. Quigley, J. Sharples, M. Walkington, and S. Wilcox for participating in the cruise and collecting this dataset. Thanks are due to the Master and crew of the RV *Lavrentyev* for their help.

References

- Bailey, R.J., D. Roemmich, G. Meyers, W. Young, and B. Cornuelle, 1993: Transports of the major current systems in the Tasman Sea. In: Karoly, D., and R. Rosen, ed., Fourth international conference on southern hemisphere meteorology and oceanography, American Meteorological Society, Boston, p.535.
- Boland, F.M., and J.A. Church, 1981: The East Australian Current 1978. *Deep-Sea Res.*, 28A, 937–957.
- Hamon, B.V., 1965: The East Australian Current, 1960–64. *Deep-Sea Res.*, 12, 899–921.
- Ridgway, K.R., and J.S. Godfrey, 1994: Mass and heat budgets in the East Australian Current: A direct approach. *J. Geophys. Res.*, 99, 3231–3248.
- Warren, B.A., 1973: Transpacific hydrographic sections at Lats. 43°S and 28°S : the SCORPIO Expedition - II. Deep water. *Deep-Sea Res.*, 20, 9–38.
- Wyrtki, K., 1962: Geopotential topographies and associated circulation in the western South Pacific Ocean. *Australian Journal of Marine and Freshwater Res.*, 13, 90–105.

Table 1. Integrated volume, heat and salt transport. Positive values are for transports into the Tasman Sea; negative values indicate transports out of the sea.

	$43^\circ 15'\text{S}$	$30^\circ 5'\text{S}$	173°E	Σ
Geostrophic (Sv)	-6.6	11.9	-6.7	-1.4
Ekman (Sv)	0.4	0.1	0.1	0.6
Heat ($\text{Watts } 10^{14}$)	-1.3	6.1	-3.6	1.2
Salt (10^8 kg s^{-1})	-2.4	4.3	-2.4	-0.5

A Hydrography in the Southern Philippine Sea: From WOCE Hydrographic Programme Section PR1S and PR24

T. Kawano, Nani Hendiarti**, Yudi Anantaesana**, Yuji Kashino*, Syaefudin**, Kei Muneyama*, Michio Aoyama* and Kentaro Ando*

* Japan Marine Science and Technology Center (JAMSTEC) 2-15, Natsushima, Yokosuka, 237, Japan

** Badan Pengkajian Dan Penerapan Teknologi (BPPT) Jl. M.H. Thamrin No. 8, Jakarta, 10340, Indonesia

The southern part of the Philippine Sea is an important area. The layer from surface to 1000 dbar, comprises the North Equatorial Current, the Mindanao Current, the South Equatorial Current, the North Equatorial Counter Current, the Mindanao and the Halmahera Eddy (Lukas *et al.*, 1991). Water masses are transported and mixed by these currents and eddies. In particular, Tropical Water transported by the New Guinea Coastal Undercurrent from the Solomon Sea may largely affect the subsurface salinity distribution in this area (Tsuchiya *et al.*, 1989). However, the north-western limit of this water has not been investigated well.

In the deep layer of the North Pacific, Antarctic Bottom Water flows northward as a bottom western boundary current (*e.g.* Stommel and Arons, 1960). This current flows from the Southern Pacific Basin to the Central Pacific Basin through the Samoan Passage and from the Central Pacific Basin to the North Pacific basin through the Wake Island Passages. Johnson and Toole (1993) described the flow of the Lower Circumpolar Water and the North Pacific Deep Water at 10°N. Their estimated net transport of the Lower Circumpolar Water was 5.8 Sv (northward) in the east Mariana Basin and 8.1 Sv (northward) in the Central Pacific Basin.

The flow from the central part of the Pacific Basin to the Philippine Basin was studied by Kaneko and Teramoto (1985). They suggested that deep water flows into the Philippine Basin through a gap called Yap-Mariana Junction. Uehara *et al.* (1993) observed at 12°N and 13°N the existence of cold and saline abyssal water between the Mariana Ridge and the Kyushu-Palau Ridge. This result provides evidence of a flow into the Philippine Sea through Yap-Mariana Junction. Using the data of GEOSECS, INDOPAC and VEGA, Gamo (1993) shows that the chemical characteristics of the Philippine Sea Bottom Water deviated significantly from the trends of the main northwestern Pacific Bottom Water although they have a common source in the central Pacific Basin bottom water. He suggested that the topographic barrier of the Izu-Bonin-Mariana Ridge sequence plays a dominant role in characterizing the Philippine Sea deep water.

In this study, we analyze data of the 1994 Kaiyo WOCE cruise, which covers the southernmost part of the Philippine Sea. We focus on the Tropical Water transported from southeast in the subsurface layer and the characteristics of the deep water in this area. Furthermore, we will discuss the possibility that the deep water of the

Western Caroline Basin flows into the Southern Philippine Basin through the sills on the Kyushu-Palau Ridge around 4°N and 5°N.

Observations

The cruise took place between the 12 February and 3 March 1994. It occupied the WHP sections PR1S and PR24. PR23 measurements were made along a section at 6°N. Fig. 1 shows the location of the stations. The station intervals on PR1S and PR24 were 20 nm or less. From 7°N, 130°E to 6°N, 127°E (called section 6°N) they were about 30 nm. Deepest samples were taken between 7–50 m above bottom. We used a Sea-Bird 'SBE911 plus' CTD with altimeter and a 36 position General Oceanics 'intelligent' rosette sampler fitted with 12-litre Niskin bottles. Water samples were analyzed with a Guildline 'Autosal 8400B' for salinity, a Metrohm '716 DMS Titrimo' for dissolved oxygen and a Bran Luebbe 'TRACCS 800' (4 channel system) for 'nutrients'. The accuracy of the CTD was ± 0.001 for salinity below 2000 m depth and ± 0.002 between 500 m and 2000 m depth. The CTD temperature and pressure are accurate to $\pm 0.001^\circ\text{C}$ and ± 1 db, respectively. Details about the data and the calibration are reported in our cruise report submitted to the WHPO.

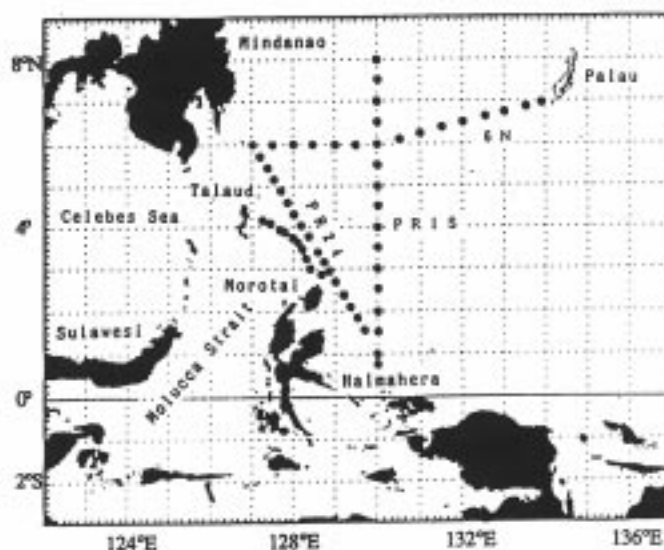


Figure 1. Location of stations.

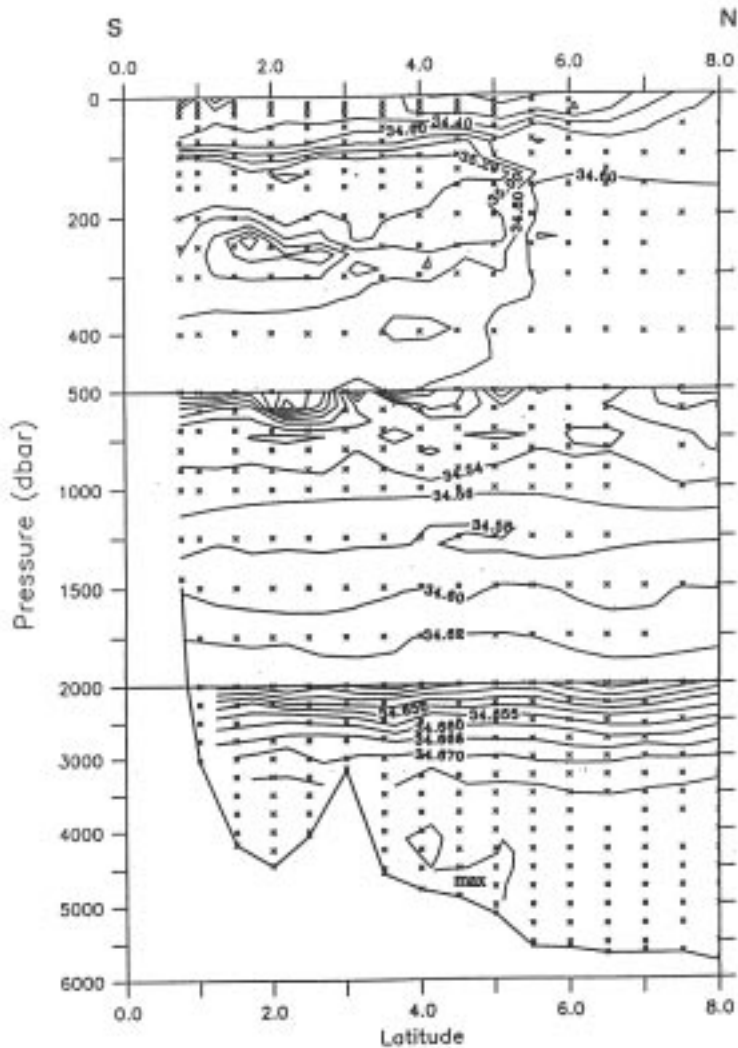


Figure 2. Vertical section of salinity along PR1S (130°E). X denotes the location where water samples were undertaken.

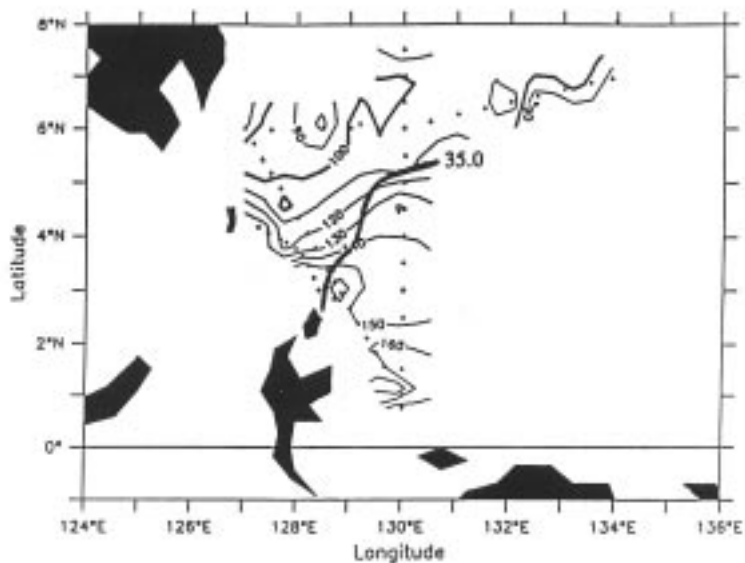


Figure 3. Horizontal distribution of pressure at $\sigma_0 = 25.0$. The thick line denotes the 35.0 salinity isoline.

Sub-surface layer

The vertical section of bottle salinities along PR1S is shown in Fig. 2. A sharp front is located at 5°N between 100 dbar and 300 dbar, with high salinities >35.00 south of the front. The salinity maximum lies at a potential density of σ_0 25.0 and is associated with a weak vertical gradient in oxygen. A similar relation was observed by Masuzawa (1968) and Tsuchiya *et al.* (1989) in sections along 137°E, 143°E and 155°E during WEPOCS-II (Fig. 16 of Tsuchiya *et al.*, 1989) and described as Tropical Water.

This fact suggests that the high-salinity water we observed south of 5°N is the same water mass as the Tropical Water of Tsuchiya *et al.* (1989).

The saline water reaches 5°N along PR1S and 4°N along PR24. Although we did not observe the velocity along PR24 directly, the velocity field can be inferred from the pressure field (Fig. 3). The large decreasing pressure gradient north of the salinity front indicates north-eastward flow. South of the front the gradient is much weaker. This makes it harder to identify the direction of the flow. But there is a possibility that the Tropical Water is entering the Indonesian Seas through Malacca Strait.

The geostrophic velocity relative to 1500 dbar along PR1S (not shown) reveals the North Equatorial Countercurrent (NECC) around 5°N above 500 dbar. The latitude of the axis of NECC coincides with the salinity front at PR1S. This result is consistent with Gouriou and Toole (1993) and indicates that the Tropical Water can be a source of not only the Equatorial Undercurrent (Tsuchiya *et al.*, 1989) but also the NECC.

Deep water properties

Table 1 shows the result of statistical analyses of the properties of the deep water (below 3000 m). The standard deviations (1- σ) of salinity and dissolved oxygen below 4000 m were small. They were only marginally higher than the precision of the measurements, while those between 3000 m and 4000 m were about 5 times as large as the precision. We could see only small differences among the three layers as shown in salinity and dissolved oxygen, however, the standard deviations of nutrients were also small. This means that the water below 4000 m is homogeneous. The properties of this homogeneous water are 34.679 ± 0.0008 in salinity, and $1.243 \pm 0.005^\circ$ in potential temperature, 150.5 ± 0.8 $\mu\text{mol/kg}$ in dissolved oxygen, 139.8 ± 1.2 $\mu\text{mol/kg}$ in silicate, 36.1 ± 0.3 $\mu\text{mol/kg}$ in nitrate and 2.47 ± 0.03 $\mu\text{mol/kg}$ in phosphate. Kawabe (1993) pointed out that the deep water north of 12°N was also homogeneous.

The values are a little bit different from those in this study. Gamo (1993) shows that the chemical characteristics of the Philippine Sea Bottom Water (PSBW) were significantly deviated from the trends of the main north-western Pacific Ocean. The homogeneous water mentioned above is also within the range of Gamo's PSBW, however it seems to be on the boundary of Gamo's definition.

Fig. 4 shows the vertical distribution of silicate concentration along section PR1S below 200 db. There is a weak minimum at 4000 db between 4°N and 5°N which coincides with a maximum in salinity (Fig. 2). Fig. 5 shows the silicate-salinity relationship below 4000 m on PR1S. The range of silicate concentration at high (34.680) salinities is from 136 to 144 $\mu\text{mol/kg}$. The lower part of this range is occupied by the stations at 4°N, 4.5°N and 5°N (triangles in Fig. 5). This water with high salinity and low silicate concentration may originate from the Western Caroline Basin because water with the same feature was not found on the PR24 and 6°N sections. According to the map of the bottom topography (JODC No. 131 and 141, 1984), the Kyushu-Palau Ridge has a sill near 4°N and 5°N. This fact supports our hypothesis of the existence of the flow into the Philippine Basin from the Western Caroline Basin.

Summary

- (1) High salinity water in the sub-surface layer coming from the southeast (which might be an extension of the New Guinea Coastal Undercurrent), reached 5°N along 130°E and also reached 4°N along the section of PR24. This fact suggests the possibility that the high salinity water originated from the southern Pacific may be transported into the Indonesian Seas through the Molucca Strait.
- (2) A homogeneous water mass lies below 4000 m in this area. The properties are 27.77 in σ_θ , $1.243 \pm 0.005^\circ\text{C}$ in potential temperature, $150.5 \pm 0.8 \mu\text{mol/kg}$ in dissolved oxygen, $139.8 \pm 1.2 \mu\text{mol/kg}$ in silicate, $36.1 \pm 0.3 \mu\text{mol/kg}$ in nitrate and $2.47 \pm 0.03 \mu\text{mol/kg}$ in phosphate.
- (3) Saline water with salinity of higher than 34.680 below 4000 m was found around 4°N and 5°N along section PR1S. The silicate concentration of this water is less than surrounding waters. Because waters with the same characteristics were not found on section PR24 and along 6°N, this water with high salinity and low

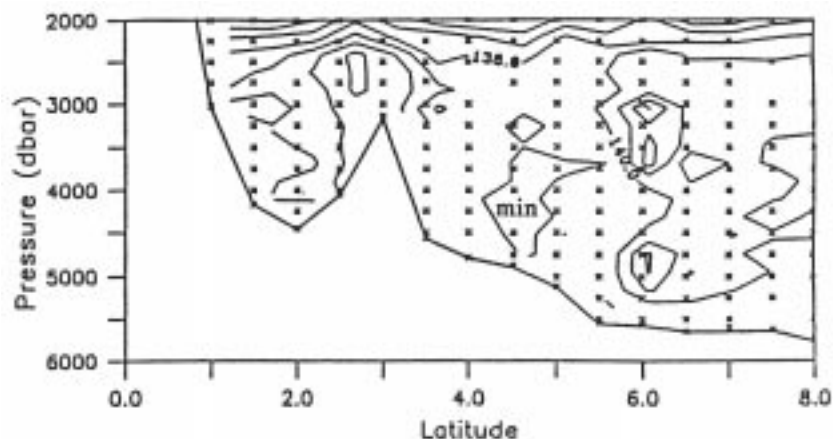


Figure 4. Vertical distribution of silicate on PR1S below 2000 dbar.

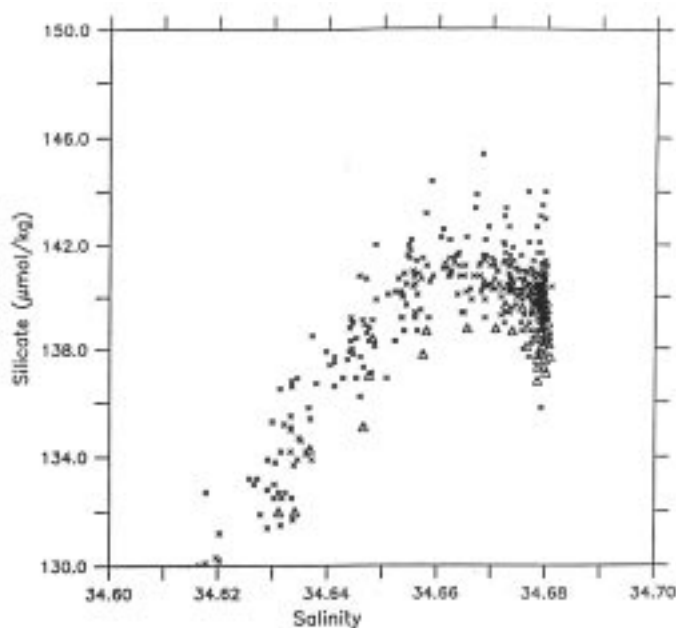


Figure 5. Silicate versus salinity along PR1S below 4000 db. Triangles denote stations at 4°, 4.5° and 5°N.

Table 1. The averages and standard deviations (σ) of the properties below 3,000 dbar

Range dbar		θ $^\circ\text{C}$	Salinity	O_2	NO_3^- $\mu\text{mol/kg}$	SiO_4 $\mu\text{mol/kg}$	PO_4^{3-}
7600-4998 ND=92	Av.	1.240	34.6794	150.64	36.08	129.7	2.46
	σ	0.003	0.0007	0.73	0.31	1.06	0.03
	%	0.23	0.0002	0.49	0.87	0.76	1.18
5003-3996 ND=151	Av.	1.245	34.6790	150.37	36.12	139.8	2.47
	σ	0.004	0.0009	0.88	0.33	1.22	0.03
	%	0.34	0.0003	0.59	0.92	0.88	1.27
4003-2998 ND=241	Av.	1.306	34.6748	146.79	36.29	140.5	2.48
	σ	0.048	0.0034	3.03	0.34	1.26	0.04
	%	3.69	0.0001	2.06	0.93	0.90	1.59

silicate values might originate from western Caroline Basin through the sill of the Kyushu-Palau Ridge near 4°N and 5°N.

Acknowledgements

The authors thank all participants of this cruise and Captain Tanaka and his crew of RV Kaiyo. This cruise was executed on the basis of the collaborative ocean research framework between Japan Marine Science and Technology Center (JAMSTEC) and Badan Pengkajian Dan Penerapan Teknologi, Indonesia (BPPT) since 1992.

A part of this research was performed through the Special Coordination Funds of the Science and Technology Agency of the Japanese Government.

References

- Gamo, T., 1993: Philippine Sea Abyssal Waters in the Northwestern Pacific: Characterization from tracer-tracer diagrams, deep ocean circulation. Physical and chemical aspects, edited by T. Teramoto. Elsevier Science Publishers B.V., 91–104.
- Gouriou, Y., and J. Toole, 1993: Mean circulation of the upper layers of the western equatorial Pacific Ocean. *J. Geophys. Res.*, 98, 22495–22520.
- Johnson, G.C. and J.M. Toole, 1993: Flow of deep and bottom waters in the Pacific at 10°N. *Deep-Sea Res.*, 40, 371–394.
- Kaneko, I. and T. Teramoto, 1985: Sea water exchange between the Shikoku–Philippine Basin and the western North Pacific Basin. Ocean characteristics and their changes, edited by K. Kajiura, Koseisha–Koseikaku, Tokyo, 54–77 (in Japanese).
- Kawabe, M., 1993: Deep water properties and circulation in the western North Pacific, deep ocean circulation. Physical and chemical aspects, edited by T. Teramoto, Elsevier Science Publishers B.V., 17–37.
- Lukas, R., E. Firing, P. Hacker, P. Richardson, C. Collins, R. Fine, and R. Gammon, 1991: ‘Observations of the Mindanao Current’ during the Western Equatorial Pacific Ocean Circulation Study. *J. Geophys. Res.*, 96, 7089–7104.
- Masuzawa, J., 1968: Second cruise of CSK, Ryofu Maru, January to March 1968. *Oceanographic Magazine*, 20, 173–185.
- Stommel, H., and A.B. Arons, 1960: On the abyssal circulation of the world ocean - II. An idealized model of the circulation pattern and amplitude in oceanic basins. *Deep-Sea Res.*, 6, 217–233.
- Tsuchiya, M., R. Lukas, R. Fine., E. Firing, and E. Lindstrom, 1989: Source waters of the Pacific Equatorial Undercurrent. *Progr. Oceanogr.*, 23; 101–147.
- Uehara, K., K. Taira and A. Masuda, 1993: Density field along 12°N and 13°N in the Philippine Sea, deep ocean circulation. Physical and chemical aspects, edited by T. Teramoto, Elsevier Science Publishers B.V., 39–49.

WOCE P19 in the Eastern South Pacific

Lynne D. Talley and Mizuki Tsuchiya, Scripps Institution of Oceanography/UCSD, La Jolla, CA 92093-0230, USA

Cruise summary

WHP section P19C along 88°E was carried out on RV Knorr between Punta Arenas, Chile, and Panama City, Panama, from 22 February to 13 April 1993. P19C was the seventh Pacific WOCE hydrographic leg on the Knorr and the fourth with basic technical support from Scripps Institution of Oceanography’s Oceanographic Data Facility (SIO/ODF). The cruise track (Fig. 1) was east of the East Pacific Rise for its entire length, and crossed four deep basins (Bellingshausen, Chile, Panama and Guatemala) separated by ridges (Sala y Gomez, Carnegie and Cocos). The track went westward along 54°S out to 88°W and then northward along 88°W and 85°50’W, up to 4°N where the track turned northwestward and then into Central America off Guatemala. This first section is an abbreviated version of the cruise report which was filed with the WOCE Hydrographic Programme Office. The complete cruise report can be obtained from the WHPO at WHOI or through anonymous ftp to sam.ucsd.edu in subdirectory pub/p19 which also includes postscript files for some of the basic

vertical sections. Section 2 is a very brief description of some hydrographic features found along the section.

All stations were to within 10 metres of the bottom and included a rosette/CTD cast. Basic station spacing was 30 nm, closing to 20 nm for 3°S – 1°S and 1°N – 3°N, and to 10 nm for 1°S to 1°N. Station spacing at the Chilean and Guatemalan coasts and over the Sala y Gomez Ridge (about 25°S) was less than 30 nm and dictated by topography. Sampling included 108 CTD/rosette stations, 13 large volume sampling (Gerard barrel) stations, and 20 200-metre bio-optics stations (J. Marra of LDEO for JGOFS). Sampling was done with a 36-place General Oceanics pylon on a rosette frame with 10-litre bottles and a CTD, transmissometer, altimeter and pinger. An RDI lowered acoustic doppler profiler (Eric Firing) was mounted inside the rosette frame for 94 stations.

The CTD data stream consisted of elapsed time, pressure, two temperature channels, conductivity, oxygen, altimeter and transmissometer signals. There were no major problems with the CTD measurements. Most of the few problems in conductivity resulted from biological

fouling of the rosette/CTD during the cast.

Water samples were collected for analyses of salt, oxygen, silica, phosphate, nitrate and nitrite on all stations and of CFC-11, CFC-12, helium-3, helium-4, tritium, AMS ^{14}C , pCO_2 , and total dissolved inorganic carbon on selected stations.

Discrete salinity, oxygen and nutrient values were compared with preliminary data acquired on P17E (Swift, chief scientist, RV Knorr) and P6 (Bryden, chief scientist, RV Knorr), and with data from the 1989 Moana Wave cruise at $9^{\circ}30'\text{N}$ and the two old 1968 Scorpio sections at 43°S and 28°S . A complete version of the comparisons, with figures and tables, can be found in the WHP P19C cruise report available from anonymous ftp. Salinity accuracy is within WOCE requirements on P19C and the

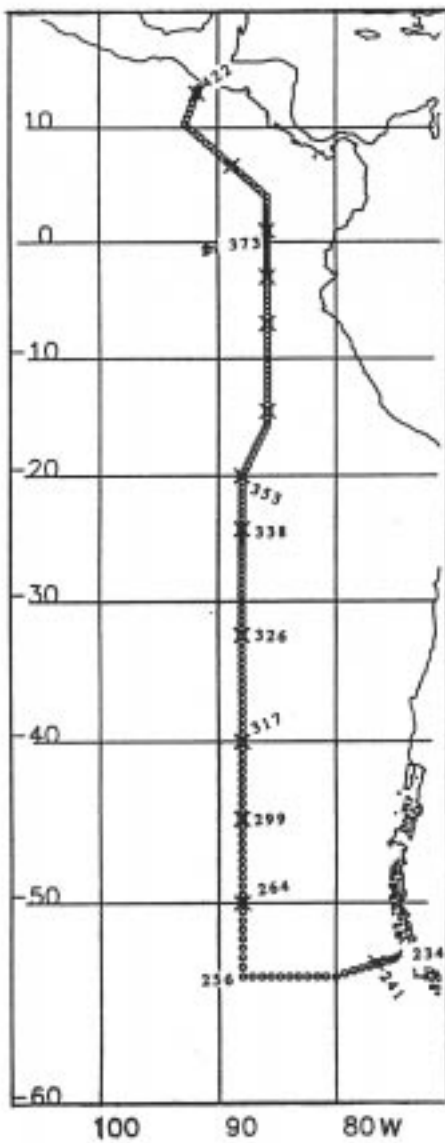


Figure 1. Cruise track for WOCE P19C (RV Knorr 138-12), 22 February 1993 – 13 April 1993. Rosette/CTD stations (circles). Large volume plus rosette/CTD station (crossed circles).

other recent cruises. There are offsets in oxygen amongst the recent cruises which are larger than the precision required but within the accuracy limits, so indicating no fundamental problems. In nutrients however, there may be inter-group differences which exceed the WHP requirements for accuracy.

CTD/rosette station times are shown in Fig. 2. These times are comparable to those from two previous Knorr WOCE legs. These numbers do not include start and stop times, so actual stations times were about 5 minutes longer. Wire speeds were generally 60 metres/minute for downcasts and 70 metres/minute for upcasts; because of stops for bottle trips and slower speeds in the upper 200 metres, the average wire speed for all stations was 55–58 metres/minute.

Towards the end of the cruise, we started to wait for a few ship rolls before closing bottles in the strong near-surface pycnocline in order to flush the bottle, as suggested long ago by Ray Weiss of SIO. This reduced the differences in CTD and bottle conductivity by two to three orders of magnitude. This suggests that the concept of closing bottles “on the fly” may result in degradation of CTD calibration, particularly in the pycnocline.

Large-volume sampling (R. Key of Princeton) was made with use of 270-litre Gerard barrels for analyses of ^{14}C , salinity, oxygen and nutrients on 13 stations. All covered the water column below 1000 metres. ^{14}C samples were collected from the rosette for the upper 1000 metres for analysis by AMS.

Underway measurements included Acoustic Doppler Current Profiling (Eric Firing of U. Hawaii), pCO_2 , pN_2O (R. Weiss, SIO), and the various variables of Knorr’s IMET system (surface water temperature and conductivity, oxygen, meteorological parameters, GPS navigation, ship’s speed and heading). Underway bathymetry was recorded every 5 minutes from the Knorr’s PDR for our own use in constructing vertical sections and as additional input to the overall data-base (S. Smith - Geological Data Center at SIO).

Twenty-one subsurface ALACE floats were deployed for R. Davis of SIO. The ballast pressure for the floats was 800 to 850 dbar. Six surface drifters were deployed for P. Niiler of SIO.

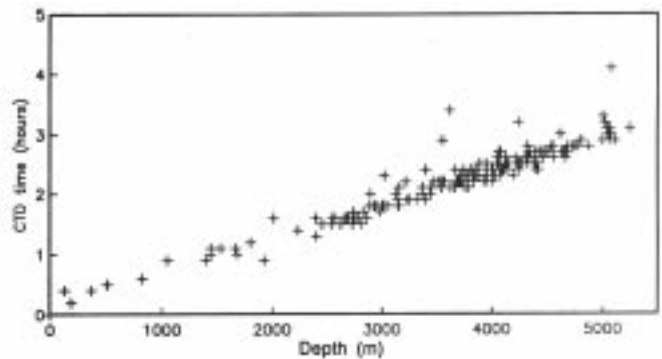


Figure 2. CTD station times (from launch to recovery, not including additional deck time).

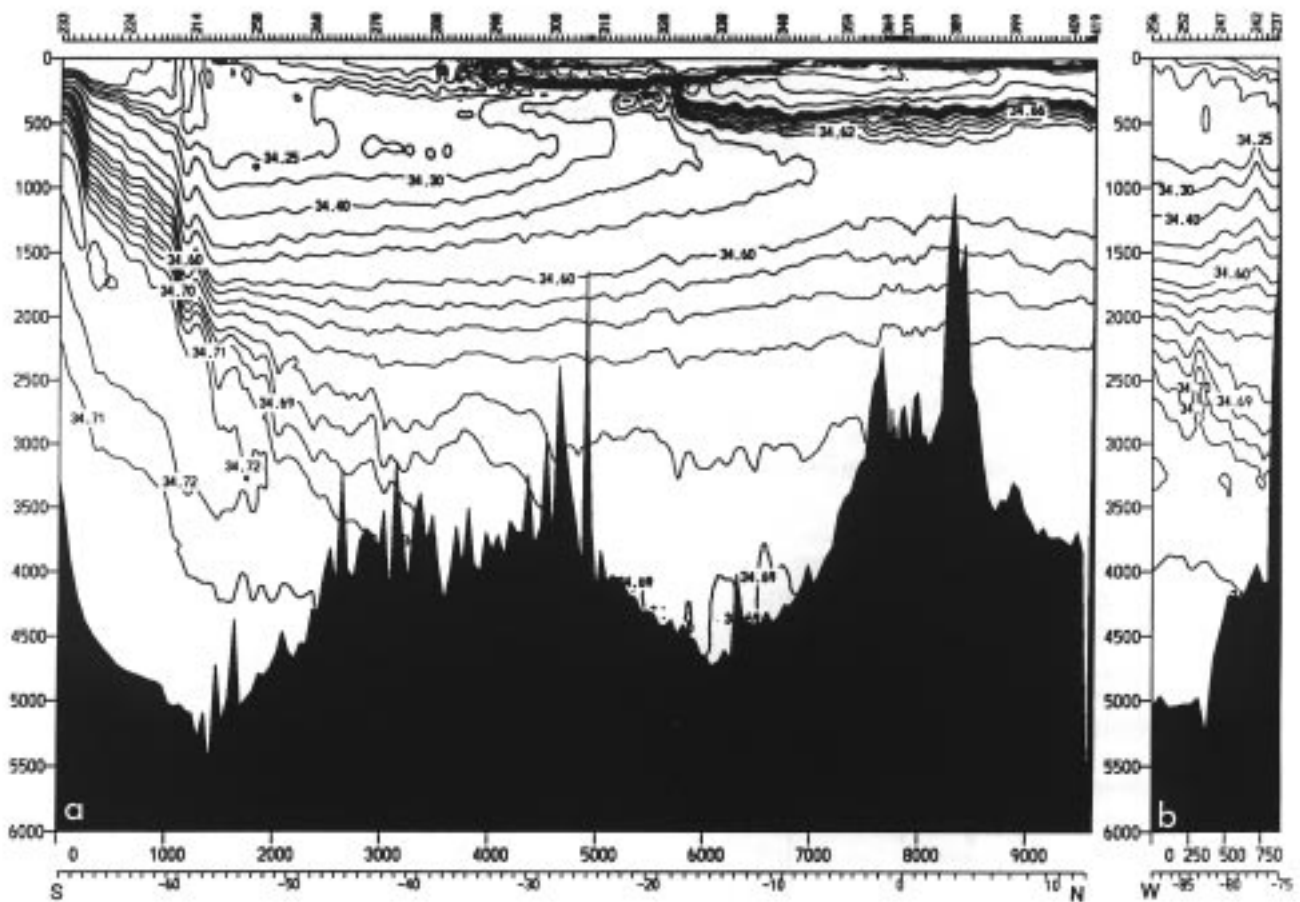


Figure 3. Vertical section of salinity along (a) 88°W and (b) 54°S from 88°W to South America. The portion of 88°W south of 54°S was collected by J. Swift of SIO on the previous WOCE leg on the RV Knorr.

Preliminary results

Vertical sections of potential temperature, salinity, oxygen and silica illustrate some of the major water mass features encountered along 88°W and eastward along 54°S. The 88°W section was extended southwards in Figs. 3 and 4 with the stations collected on the preceding leg by Swift (see article in International WOCE Newsletter No. 18), which are used here with his permission.

1. The major Pacific water masses on the section were Antarctic Intermediate Water (stability and salinity minimum/oxygen maximum at 400–600 metres), Pacific Deep Water (oxygen minimum at 1500–2000 metres and silica maximum at about 2800 metres), North Atlantic Deep Water or Upper Circumpolar Water (salinity maximum at about 3500 metres), and Antarctic Bottom Water or Lower Circumpolar Water (oxygen maximum and salinity minimum at the bottom). At the top of the Chile Rise, between 43° and 41°S, the Antarctic Bottom Water and Circumpolar Water disappeared and did not reappear as we crossed into the western portion of the Chile Basin. The Chile Basin was filled to the bottom with a much more homogeneous water mass than in the Bellingshausen Basin, with high silica, low oxygen and relatively

warm water (greater than 1.4°C). The sill depth for the Chile Basin appears to be at about 3500 m. The bottommost waters in the Chile Basin have higher oxygen and lower silica than those above, indicating southern origin.

2. At 54°S off the coast of Chile there was a clear eastern boundary regime of about 500 km width at 54°S, extending to the ocean bottom. Characteristics of this regime are relatively low oxygen in the Pacific Deep Water oxygen minimum, relatively low salinity in the Circumpolar Water salinity maximum, relatively high silica in the Pacific Deep Water silica maximum, and potential vorticity signatures for these water masses which also indicate an eastern boundary regime. Properties in this eastern boundary region match fairly well with those found at the northern side of the Bellingshausen Basin, between about 45 and 50°S. Large-scale currents are therefore probably southward to the bottom along the eastern boundary, out to 81°W. They are also eastward along 88°W at the northern side of the Bellingshausen Basin, indicating cyclonic flow in accord with Reid (1986).
3. The near-surface waters in a large patch west of southern Chile (54°S, 79°W up to 52°S, 88°W) were very similar to Antarctic Intermediate Water (AAIW).

The salinity minimum was nearly non-existent in this outcrop region and the oxygen in the pycnostad was at the surface value. The density of the thick pycnostad was $27.01 \sigma_\theta$. This was only slightly less dense than the well-defined salinity minimum AAIW found east and north of the patch ($27.02 \sigma_\theta$). A well-defined oxygen maximum was also found in the AAIW east and north of the patch. Dynamic height at the surface relative to deeper levels was essentially flat throughout the patch, rising both to the east and to the north, suggesting a broad cyclonic flow around it of waters which then enter Drake Passage. This suggests that the local Subantarctic Mode Water in the southeastern Pacific is essentially identical to the AAIW which spreads northward, probably by subduction, in the eastern South Pacific.

The low potential vorticity signature of the AAIW was found as far north as about 30°S . The well-defined oxygen maximum associated with the AAIW is found as far north as about 24°S . The salinity minimum of course extends to the northern end of the section in the North Pacific off Guatemala. The density of the salinity minimum shifts rapidly from about $27.1 \sigma_\theta$ to $27.3 \sigma_\theta$ between 20° and 17°S . There is significant fine structure (interleaving) at the

minimum between about 23°S and 17°S . The highest salinity AAIW is found in the equatorial region and north of the equator. Oxygen in the equatorial AAIW is 0.5 ml/l higher than under the low oxygen regimes 10° south and 5° north of the equator.

4. Low salinity surface water extending westward from South America centred at about 40°S was evident in prior work, and has been called the Deacon jet. This fresh water was very clearly defined along 88°W between 54°S and 34°S , with an abrupt front at the northern edge. Changes in dynamic height at the surface relative to deeper levels suggest eastward flow throughout the low salinity tongue, despite the apparent source of the lowest salinity water to the east, based on historical data. It extends down to about 200 metres and is the apparent source of the shallow salinity minimum found in the northern subtropical gyre of the South Pacific. The shallow salinity minimum is evident on this section between 38°S and 20°S .
5. There was an isopycnal uplift at station 242, at 54°S , 77°W , in the upper 1500 metres, accompanied by even stronger uplift of properties. This suggests a cyclonic flow around the rise offshore of the Chile Trench.

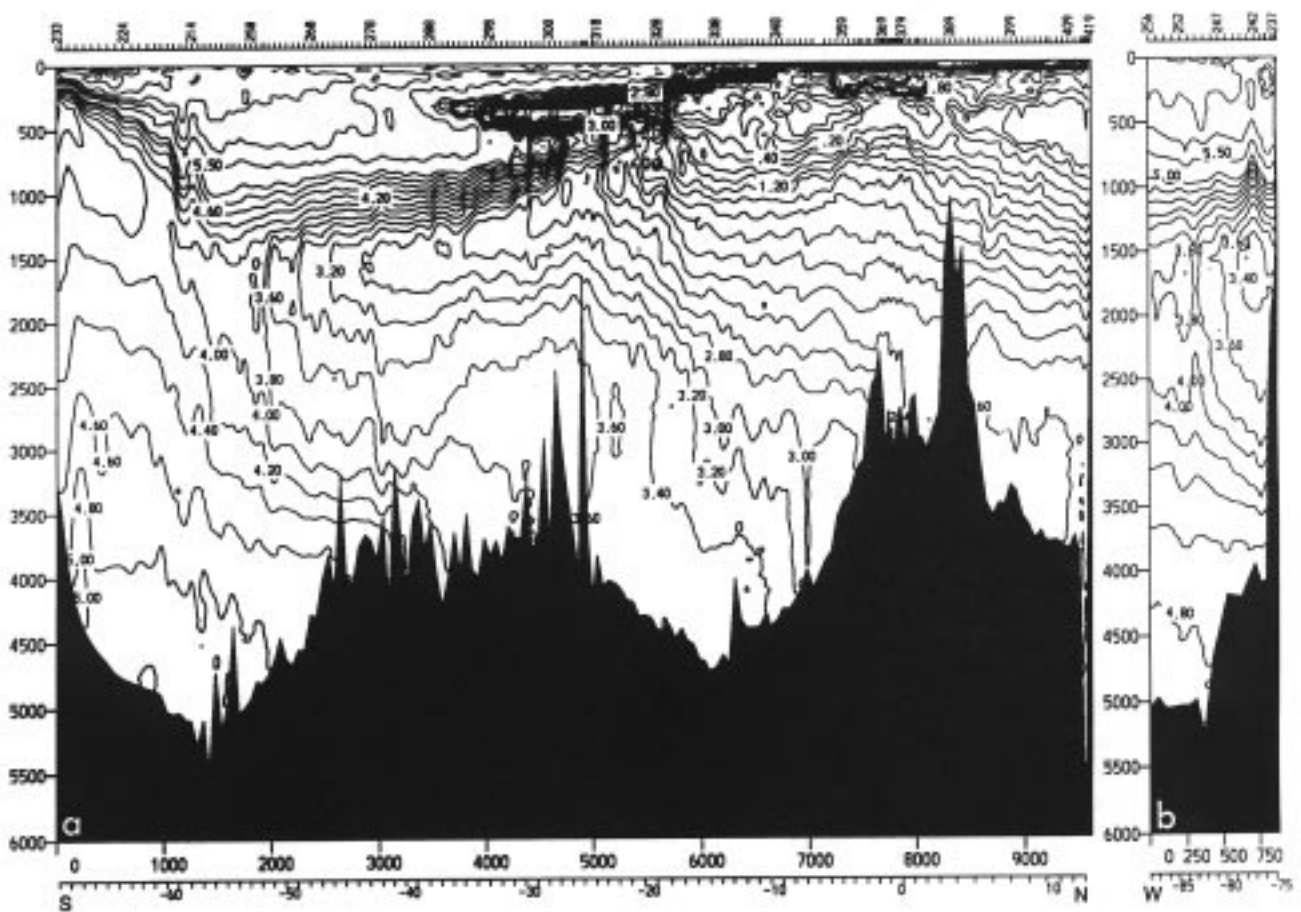


Figure 4. Vertical section of oxygen (ml/l) along (a) 88°W and (b) 54°S from 88°W to South America.

6. The high salinity northern subtropical surface water penetrates to about 200 metres depth between its onset near 38°S up to about 20°S (northern limit of the underlying salinity minimum). North of this, the higher salinity influence plunges down to about 500 metres, and north of about 12°S there is a well-defined sub-surface salinity maximum at about 100 metres depth.
7. The section crossed the equator in the deepest part of the narrow region between the Galapagos Islands and South America. The maximum depth here was around 3000 metres. This is an active geothermal region. Centred about the equator the bottom water was noticeably warmer (by 0.3°C) than on either side of the bathymetric rise, and quite uniform over about 700 metres from the bottom. This uniform bottom layer was also more uniform in oxygen and salinity than on either side of the equator, indicating mixing. The equatorial band (within 2° of the equator) also has striking vertical structure from 500 metres to the

ocean bottom, evidenced in an increase in layering as quantified by minima and maxima of Vaisala frequency, compared with the more monotonic structure farther from the equator.

8. The oxygen minima north and south of the equator in this region are notable for the very low values of oxygen very close to the surface (less than 0.02 ml/l). The oxycline separating the surface saturated layer from the underlying minimum layer lies at about 50 metres depth. A double nitrite maximum is found associated with the oxygen minima north and south of the equator: south of the equator the deeper nitrite maximum is at about 150 metres and north of the equator it is centred at 400 metres.

Reference

- Reid, J.L., 1986: On the total geostrophic circulation of the South Pacific Ocean: flow patterns, tracers and transports. *Prog. Oceanogr.*, 16: 1-61.

WOCE Observations in the Pacific Ocean

N.P. Holliday, WOCE IPO

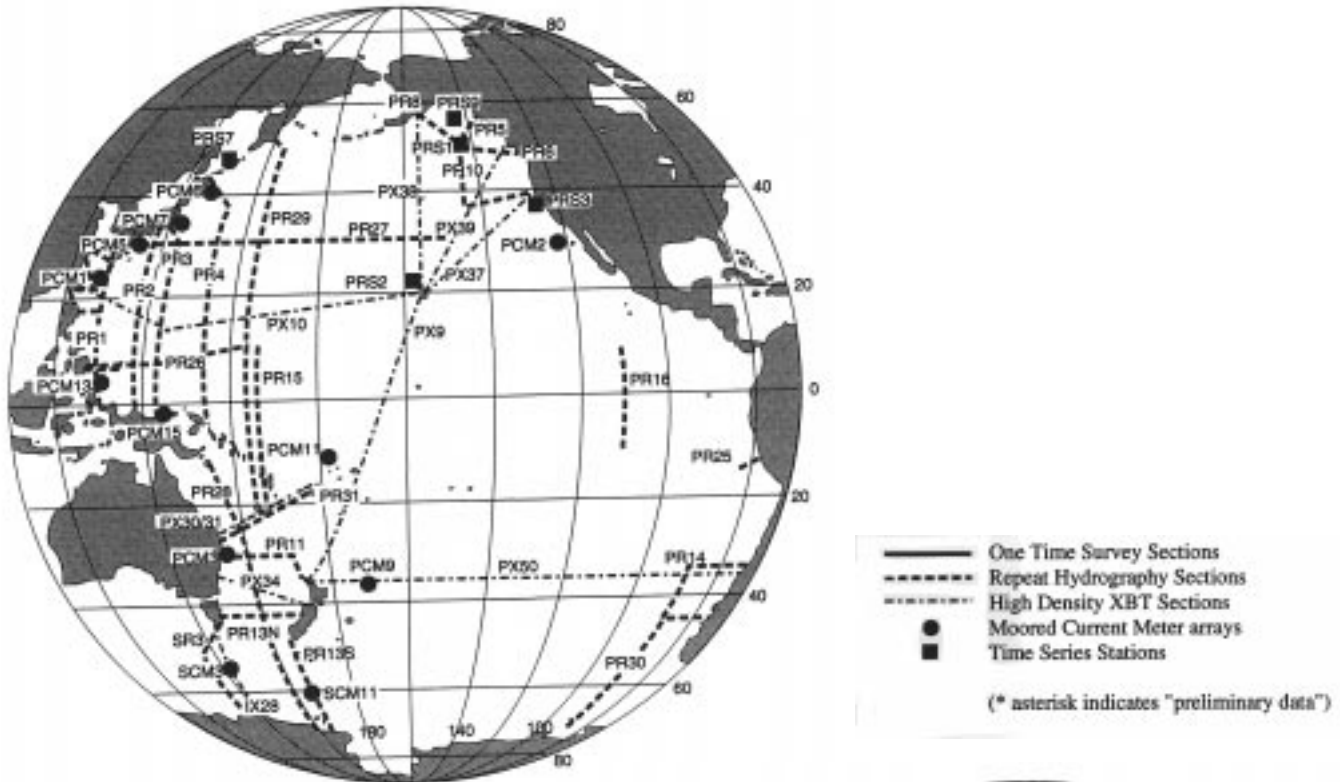
During the years 1991–1994 the Pacific Ocean was subjected to an intensive one-time survey resulting in the grid of sections illustrated in Fig. 1. Repeated hydrographic sections, time series stations, current meter moorings and high density XBT sections began in 1990 and will continue to monitor the Pacific through 1997. Fig. 2 shows schematically where the continuing observations are. Absent from Fig. 2 are the low density XBT sections, subsurface floats, surface drifting buoys and sea level stations which will also continue throughout the WOCE Field Phase.

Providing WOCE data and products to a large science community in a timely way is a central aim of WOCE, in order that the data from individual sections and projects can be included in the wider synthesis of WOCE data. Many of the data sets collected since 1990 should now be in the public domain but still



Figure 1. Completed Pacific Ocean One Time Survey Sections.

Figure 2. Committed and Ongoing Pacific Ocean Observations (excluding One Time Survey, Floats, Drifters, Sea Level Stations and Low Density XBTs).



remain with individual investigators, including data from 96 Pacific hydrographic sections and 5 Pacific current meter arrays. Fig. 3 illustrates the Pacific sections, stations or arrays from which data are now publicly available (excluding low density XBT sections, drifters and sea level stations, many of which are available in real or near real time, and subsurface floats). The P1, P3 and P4 one time survey sections are pre-WOCE but will not be repeated. All other one-time survey and most repeat section data now available are "preliminary", *i.e.* have not yet completed the Data Quality Evaluation process but have been released with the permission of the principal investigators (indicated on Fig. 3 with an asterisk). For more information about any WOCE field programme activities, contact the WOCE Data Information Unit (DIU). Details of how to contact the DIU and how to obtain WOCE data are given on page 35 of this Newsletter.



Figure 3. Elements of the Pacific Field Programme from which Data are now Publicly Available (excluding Floats, Drifters, Sea Level Stations and Low Density XBTs).

Intense Mixing of Antarctic Bottom Water in the Equatorial Atlantic

Kurt Polzin, University of Washington, School of Oceanography, Seattle, WA 98195; Kevin Speer, Laboratoire de Physique des Océans, IFREMER, 29280 Plouzané, France; John Toole and Ray Schmitt, Woods Hole Oceanographic Institution, Woods Hole, MA 02543, USA

The Mid-Atlantic Ridge represents a formidable barrier to the spread of Antarctic Bottom Water (AABW) in the Atlantic. Formed in the Weddell Sea and modified in the Southern Ocean, AABW is confined by bathymetry to the western basins of the South Atlantic as it moves north. Sharp property gradients are found in the western basins as Antarctic Bottom Water intrudes north underneath the warmer and saltier North Atlantic Deep Water. In contrast, the densest waters in the eastern basins of the Atlantic are renewed by a relatively small cumulative transport of bottom water through a handful of small gaps in the Mid-Atlantic Ridge. The eastern basin's water properties consequently have much smaller vertical and horizontal gradients.

One of the primary conduits of bottom water across the Ridge is the Romanche Fracture Zone (RFZ), a large offset of the ridge straddling the equator, Fig. 1. The bottom water flow through the fracture zone supplies the abyssal waters of the Sierra Leone Basin to the north and the Guinea and Angola Basins to the east and south. The main (shallowest) sill in the passage is located just north of the equator near 0°42'N, 14°42'W. Mercier *et al.* (1994) established its depth to be 4350 m. The Chain Fracture Zone, which lies immediately to the South, has a significantly shallower sill (4050 m, Mercier *et al.*, 1994) and bottom

water transport is expected to be small relative to that through the Romanche.

Recent hydrographic work regarding the RFZ has suggested substantial transport through this channel and the importance of both blocking and mixing effects. Mercier and Bryden (1994) estimated the flow of bottom water through the Romanche Fracture Zone from hydraulic theory and an assumed level of no flow coinciding with the 2.1°C potential temperature surface. They predicted a velocity at the main sill of 0.37 m s⁻¹, and a net bottom water transport of 2.4 x 10⁶ m³ s⁻¹. Negligible uplift of the deepest isotherms (and isopycnals) were observed over the main sill of the RFZ, suggesting that waters in the western Atlantic below the main sill depth were physically blocked from entering the eastern Atlantic. Hydrographic survey data by Mercier *et al.* documented bottom potential temperature at the main sill to be 0.920°C. Significantly, they report bottom temperatures in the Sierra Leone Basin to the north-east of approximately 1.5°C, more than 0.5°C warmer. This indirect evidence of significant mixing within the RFZ motivated an exploratory study of the small-scale flow field and turbulence in this narrow passage.

The data in this study were primarily obtained with the High Resolution Profiler (HRP) (Schmitt *et al.*, 1988), a free-falling, internally recording profiler. The HRP is equipped with an acoustic velocimeter that senses relative horizontal flow. Estimates of the oceanic velocity profile are derived from these relative velocity data and onboard accelerometer and magnetometer measurements. Temperature, conductivity and pressure are sensed with an NBIS Mark III CTD. The HRP also carries a full microstructure suite. These sensors provide estimates of the velocity, temperature and conductivity gradient variances at centimeter scale. Twenty eight HRP fine- and micro-structure profiles were made to depths as great as 5300 m in the RFZ, two stations were occupied in the Chain Fracture Zone and 25 additional profiles were obtained in regions adjacent to RFZ. In addition, a number of CTD yo-yo and tow-yo stations were occupied.

High-resolution bathymetric maps (Fig. 2.; H. Mercier, personal communication) show the bottom water flow is clearly constrained by the northern wall of the RFZ which extends eastward

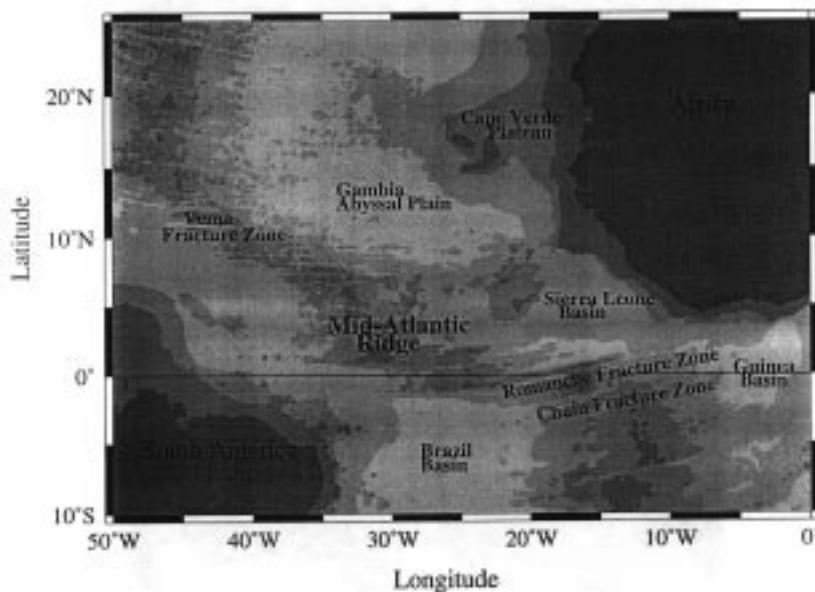


Figure 1. Bathymetry of the tropical Atlantic Ocean. Dark shading denotes shallow topography. The fracture zones represent deep valleys in the Mid-Atlantic Ridge and permit the flow of bottom water from western to eastern basins.

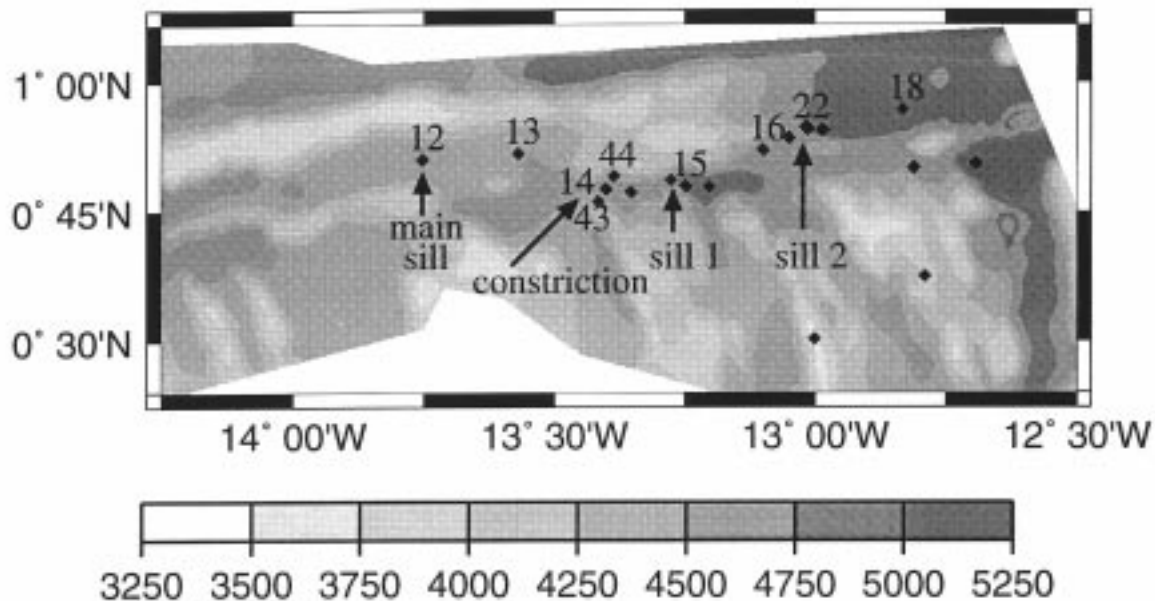


Figure 2. Bathymetry of the Romanche Fracture Zone from multi-beam depth sounder data, courtesy of H. Mercier (IFREMER) with positions of HRP stations. Numbered stations are discussed in the text.

at 0.5–1.0°N to about 13°10'W. The southern “wall” has numerous gaps which open into a region of broken topography with channels that reach south to the Chain Fracture Zone. However, flow through this “communication region” (to use Mercier *et al.*'s terminology) is thought to be small (Mercier *et al.*, 1994).

HRP work within the RFZ focused downstream from the main sill to the exit in the Sierra Leone Basin. The potential temperature field (Fig. 3a) shows the most dramatic response of the fluid is limited to the bottom water (defined as $\theta < 1.9^\circ\text{C}$, e.g. McCartney and Curry, 1993). In addition, note the reflection of a large scale pressure gradient in isotherm slopes for water with $\theta < 2.1^\circ\text{C}$. There are three regions in which the isotherms are very steeply sloped. These correspond to topographic features which influence the flow of bottom water downstream from the main sill. The first topographic feature is a constriction of the fracture zone at 0°47'N, 13°25'W. The second is a sill immediately downstream from the constriction (0°47'N, 13°18'W). The third consists of a broad sill and abrupt downslope at 0°55'N, 13°W. The bottom water can be seen to respond to the constriction and the sills by plunging to greater depths. Dramatic changes in the flow can be inferred from the sloping isotherms and an energy conservation principle (Bernoulli function). The pattern suggests that potential energy is traded for kinetic energy along the channel, implying that the flow accelerates downstream. The velocity profile data acquired by HRP (Fig. 3b) supports this idea. Immediately downstream of the sills the isotherms abruptly rise, suggesting the possibility of internal hydraulic jumps. As the flow progresses along the channel, isotherms can be seen to disappear, providing qualitative evidence of mixing processes.

The largest velocities in the RFZ are found within the bottom water (Fig. 3b). At the main sill the highest velocity observed was approximately 0.25 m s^{-1} . The acceleration implied by the steeply sloping isotherms is apparent in the velocity profiles immediately downstream of the topographic features, where velocity maxima attained values of approximately 0.50 m s^{-1} . Dive 18, although located in the deepest part of the exit channel into the Sierra Leone Basin, appears to be out of the main flow axis; profiles obtained closer to the terminus of the northern ridge wall showed much stronger bottom water velocities. As well, two profiles taken in the eastward extension of the RFZ towards the Guinea Basin found weaker flow.

The flow accelerations noted above provide for extremely large shears. The Richardson number associated with the large scale flow (estimated over a 100 m vertical scale) was below the linear instability criterion of 0.25. We believe that the strong shear associated with this flow leads to the exceptionally large turbulent mixing rates observed in these stations (see below). The fact that the RFZ sits virtually on the equator contributes to this interpretation: the large scale pressure gradient apparent in Fig. 3a cannot be balanced by the Coriolis force as at higher latitudes. Thus turbulent shear stresses must be generated to limit the down-gradient acceleration by providing a retarding force on the current. Such stresses arise in the context of both bottom boundary currents and in lee wave generation – critical layer absorption. It may also be valid to consider the site to be under internal hydraulic control.

Exceptionally large values of the turbulent kinetic energy dissipation rate (ϵ) were observed east of the main sill (Fig. 3c), particularly downstream from the topographic features discussed previously. Maximum dissipation rates,

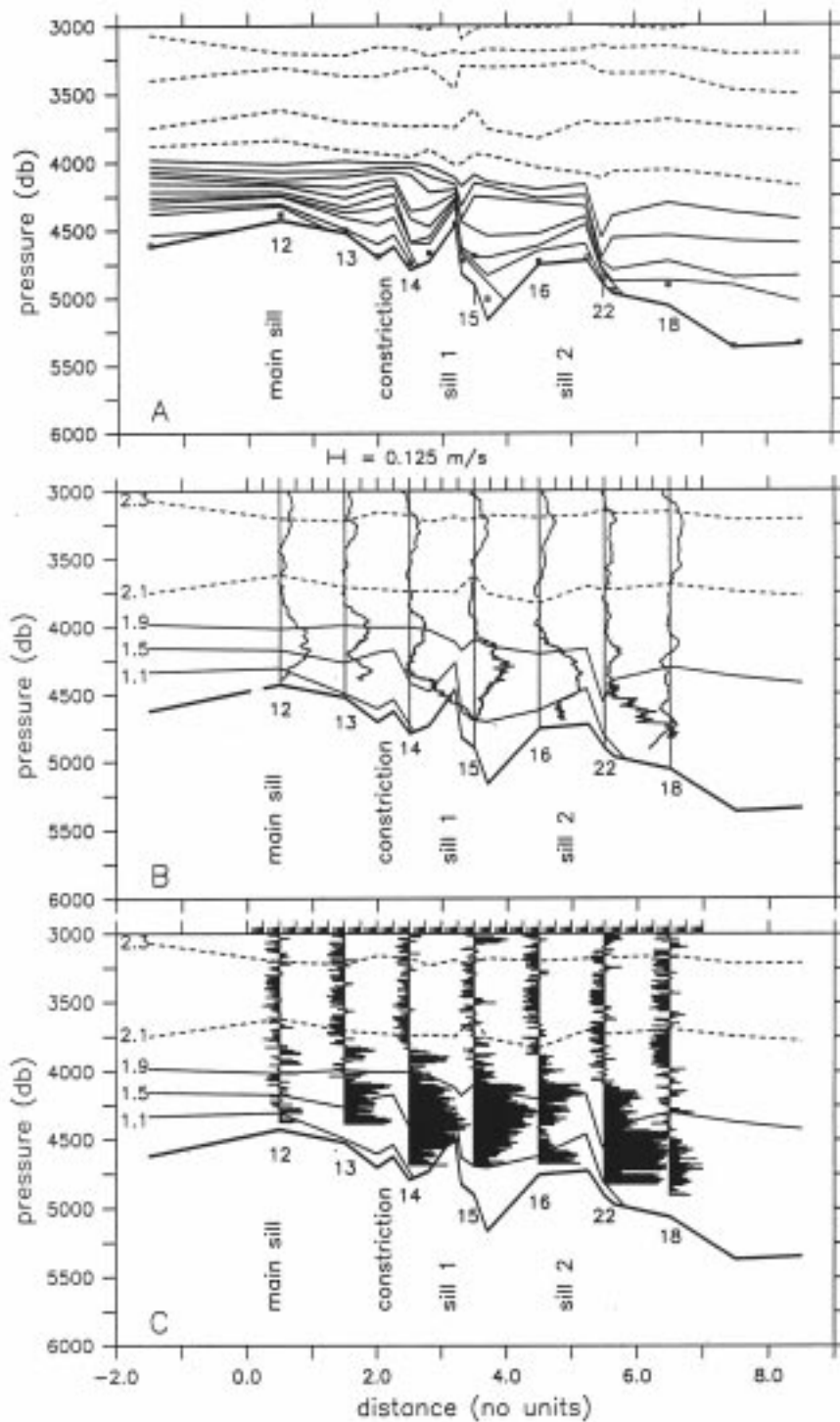


Figure 3. Along channel sections of (a) potential temperature, (b) velocity and (c) turbulent dissipation. In order to enhance the clarity of the presentation, the separation between stations is approximate. The section spans 160 km. For HRP station numbers see Fig. 2. (a) The contour interval is 0.1°C . Solid contours represent $\theta \leq 1.9^{\circ}\text{C}$ (i.e. bottom water). The symbols correspond to the greatest pressure attained by either the HRP or a contemporaneous CTD profile. Additional data from CTD work completed in 1991 by H. Mercier and K. Speer (Mercier et al., 1994) are included to refine the picture. The earlier data are virtually identical to the present data in the case of co-located data (e.g. bottom potential temperatures vary by only 0.02°C). (b) The velocity profiles have rotated into along- and across channel coordinates and referenced by setting the velocity at the depth of the 2.1°C potential temperature isotherm to zero. The velocity scale appears above the figure. (c) Note the logarithmic axis. The dissipation data is 'referenced' to a value of 10^{-10} W/kg. That is, values of ϵ greater than 10^{-10} appear as a horizontal line to the right of the vertical.

in excess of 1×10^{-6} W/kg, were observed just past the second sill (site of dive 22), where consistently large values of dissipation were found in a series of repeated profiles. The heightened levels of turbulence were generally constrained to be within the bottom water. However, this was not exclusively the case, as evidenced by dive 22 at the second sill. The turbulent dissipation rate was relatively small at the top of the main sill (profiles 12 and 13). Along with the negligible uplift of the deepest isotherms upstream of the main sill, these relatively small dissipation rates imply that the flow of water colder than 0.9°C is simply blocked.

The eddy diffusivity for stations appearing in Fig. 3c has been computed using the method of Osborn (1980):

$$K_p = \gamma \epsilon / N^2.$$

A mixing efficiency, γ , of 0.2 was assumed. The average K_p below 4000 db is $150 \times 10^{-4} \text{ m}^2 \text{ s}^{-1}$. This contrasts with estimates of the mid-depth diffusivity at these and other stations in the region of $0.2 \times 10^{-4} \text{ m}^2 \text{ s}^{-1}$. A note of caution is in order. It is possible that we may not have sampled hot spots with much greater turbulent intensification. We intend to make estimates of water mass conversion rates based on velocity and temperature observations to compare with the microstructure measurements.

A cross-channel section consisting of three profiles (14, 43 and 44) was occupied just downstream of the constriction ($13^{\circ}25' \text{ W}$) in order to estimate the transport of bottom water, Fig. 2. At this site the average depth of the 1.9°C potential temperature surface defining the top of the bottom water is approximately 3940 m. The channel on this section has a maximum depth of 4707 m. The northern channel wall along the section line rises to approximately 4050 m, reaches a plateau, then rises again to depths shallower than 4000 m. To the south, the channel wall is formed by a ridge which extends in the southeast direction. Along the section line the bathy-

metry rises to only 4200 m at the ridge crest, but following the ridge axis southeast the bottom also shoals to well under 4000 m depth. Our sampling pattern thus defines well the flow of the densest waters through the RFZ (those waters below about 4200 m) but the upper portion of the bottom water is not well constrained by these observations. Confining the integration of the velocity profiles in the horizontal by the 4050 m depth contour to the north and the 4200 m contour to the south, we obtain a transport of $1.0 \times 10^6 \text{ m}^3 \text{ s}^{-1}$ assuming a zero velocity surface at the 2.1°C potential temperature surface (as taken by Mercier and Bryden, 1994). By extrapolation, we estimate possible additional contributions of $0.2 \times 10^6 \text{ m}^3 \text{ s}^{-1}$ to the North and $0.1 \times 10^6 \text{ m}^3 \text{ s}^{-1}$ to the South.

This total transport estimate is less than that which has been previously estimated by Mercier and Bryden ($2.4 \times 10^6 \text{ m}^3 \text{ s}^{-1}$). At the main sill we observed a maximum bottom water velocity of about 0.25 m s^{-1} , less than the 0.37 m s^{-1} prediction of Mercier and Bryden. Downstream, the maximum along channel velocity estimates were in excess of 0.50 m s^{-1} , but the area averaged velocity over the domain occupied by bottom water was significantly less (0.17 m s^{-1}). This velocity difference with Mercier and Bryden is partially compensated in the transport estimates by the respective values of bottom water layer thickness. Mercier and Bryden took a bottom water thickness of 320 m at the main sill. The horizontally averaged layer height at the downstream section is 500 m. The last discrepancy is with channel width; Mercier and Bryden assumed a rectangular cross-section of 20 km width. At the HRP section the vertically averaged channel width is 8 km.

Our transport estimate is bounded by previous indirect estimates. Warren and Speer (1991) and Schlitzer (1987) suggested relatively high transport rates (2 and $2.6\text{--}5.1 \times 10^6 \text{ m}^3 \text{ s}^{-1}$, respectively). McCartney and Curry (1993) placed an upper bound on the transport of $1.2 \times 10^6 \text{ m}^3 \text{ s}^{-1}$. While flow along the RFZ may exit into the communication region before it reaches the HRP section line, Mercier *et al.* suggest this flow to be small and directed northward, not southward. Our measurements in the deep valleys of the communication region support their inference of weak flow. In addition, transport through the Chain FZ (estimated from profiles at 43°S , $12^\circ50'\text{W}$ and 37°S , $12^\circ24'\text{W}$) appears quite small relative to the transport in the Romanche. The present measurements argue for a low transport of bottom water.

Vertical mixing is required in order to complete the upwelling limb of the thermohaline circulation. This process is most apparent in narrow passages such as the Romanche Fracture Zone where striking changes in water mass properties are evident. The exceptionally high levels of turbulent dissipation found here contrast dramatically with low mixing rates determined from microstructure measurements in the abyssal interior (Toole *et al.*, 1994). The unique measurements presented here allow us to quantify the process of water mass conversion and understand the mechanisms behind it. Within this sill environment, the turbulence appears linked to the

acceleration of the bottom water in response to variations in topography. As the bottom water accelerates, the shear between it and the overlying waters appears to become unstable, causing intense turbulence in the bottom-most 500 m of the RFZ. As a consequence, the coldest waters exiting the RFZ and entering the Sierra Leone Basin are fully half a degree warmer than those flowing over the main RFZ sill. Thus, turbulent mixing appears to be as important as blocking by sills in setting the bottom water characteristics of the Atlantic Ocean's eastern basins. This is one of the best examples of how ocean turbulence at scales as small as 1 cm can influence major-ocean-basin water properties. Accurate parameterization of these mixing processes, key to achieving realistic models of ocean circulation, remains an important problem in physical oceanography.

Acknowledgements

We would like to acknowledge the essential contributions of E. Montgomery, D. Wellwood and T. Bolmer to HRP operations, J.-P. Girardot and T. Penduff for CTD work, N. Oakey (BIO) for shear probe calibration assistance and advice, and Le Noroit Commandant G. Trédunit and his crew for skillful ship handling. This work was funded by the U.S. National Science Foundation and the French CNRS and IFREMER.

References

- McCartney, M.S. and R.A. Curry, 1993: Transequatorial flow of Antarctic Bottom Water in the western Atlantic Ocean: abyssal geostrophy at the equator. *J. Phys. Oceanogr.*, 23, 1264–1272.
- Mercier, H., and H. Bryden, 1994: Flow of Antarctic Bottom Water over the sill in the Romanche Fracture Zone. *WOCE Newsletter*, 17, 9–11.
- Mercier, H., K.G. Speer, and J. Honnorez, 1994: Pathways of bottom water through the Romanche and Chain Fracture Zones. *Deep-Sea Res.*, in press.
- Osborn, T.R., 1980: Estimates of the local rate of vertical diffusion from dissipation measurements. *J. Phys. Oceanogr.*, 10, 83–89.
- Schlitzer, R., 1987: Renewal rates of east Atlantic deep water estimated by inversion of ^{14}C data. *J. Geophys. Res.*, 90, 2953–2980.
- Schmitt, R.W., J.M. Toole, R.L. Koehler, K. Doherty, and E. Mellinger, 1988: The development of a fine- and microstructure profiler. *J. Atmos. Oceanic Technol.*, 5, 484–500.
- Toole, J.M., K.L. Polzin, and R.W. Schmitt, 1994: Estimates of diapycnal mixing in the abyssal ocean. *Science* 264, 1120–1123.
- Warren, B.A., and K. G. Speer, 1991: Deep circulation in the eastern South Atlantic Ocean. *Deep-Sea Res.* 38 (supplement), s281–s322.

One-time Section A23 Completed on RRS James Clark Ross Cruise 10

Karen Heywood, University of East Anglia, Norwich, UK; Brian King, IOSDL, Wormley, Surrey, UK, and the personnel on JCR Cruise 10.

RRS James Clark Ross is a combined logistics and research ship, operated by the British Antarctic Survey (BAS); at 100 metres length it is the largest of the UK research ships.

Cruise JR10 departed from Stanley, Falkland Islands on 20 March 1995, and steamed to Punta Delgada, Chile to pick up the last member of the scientific party, who has an Argentinian passport and could not enter the Falkland Islands, even for the purposes of joining the ship. The cruise ended in Rio de Janeiro, Brazil on 6 May to complete WHP one-time section A23. Although 128 stations were occupied in total, tests, repeats and overlap mean that the section effectively consists of 114 small volume stations.

Two factors combined to force the Weddell Sea segment well away from the nominal longitude for the section which was 35°W: the cruise was scheduled later in the season than the PIs requested, and the Weddell Sea ice cover was of greater extent than the climatological mean. Although the ship has considerable ice capability, the cruise schedule did not allow sufficient time to adopt a slower and more westward track; the section therefore commenced at 72°28'S, 16°32'W in 186 metres of water, about one and a half miles from the Riiser-Larsen Ice Shelf.

Throughout the southern part of the track, sub-zero temperatures and strong winds made it necessary to bring the CTD rosette into the enclosed water bottle annex to avoid freezing. Since the CFC analysts were content that indoor sampling was not leading to contamination, this practice was continued until external temperatures were substantially above zero.

Just as the section encountered the Polar and Sub-antarctic Fronts, a medical emergency required an immediate diversion to Stanley. Even at the ship's maximum speed of 15 knots the return trip took five days, after which an overlap of seven stations was required in order to join the section properly. Some benefit now resulted from being the last cruise of the season, because BAS were able to extend the cruise to restore the lost scientific time.

Disappointingly, the cruise ended as it had begun, by failing to overcome diplomatic hurdles. Negotiation for permission to make measurements in Brazilian waters failed at the last minute because we were unable to pick up a Brazilian Naval observer when the ship arrived in the vicinity of Rio de Janeiro. The presence of two Brazilian nationals in the scientific party was insufficient, and the ship was forbidden to work within 200 miles of Brazil. This means that the last station is in 2577 metres of water approaching the continental slope, and the Brazil Current has not been sampled.

The cruise report will be accessible from the A23 home page on the WWW (<http://www.mth.uea.ac.uk/ocean/a23/welcome.html>). Preliminary scientific results

are likely to be presented in the same location, as they become available. The rosette package consisted of a CTDO, plus transmissometer, fluorometer, near-bottom altimeter and 24 place GO pylon. The Niskin bottles were a mixture of GO and new FSI bottles; the latter performed quite satisfactorily. PIs responsible for selected datasets included: nutrients (R. Sanders, UEA), CFC (A. Watson, PML), CO₂ (J. Robertson, U. Southampton), O₁₈ (R. Frew, UEA), He/Tritium (C. Rueth, U. Bremen). In addition to the water sampling, 10 ALACE floats and 84 XBTs were deployed, as were twice-daily radiosondes. Underway measurements included ADCP, thermosalinograph and a comprehensive programme of surface meteorology (T. Guymmer, JRC).

A major setback occurred in mid-cruise when 3000 metres was cut off the CTD cable after it developed an electrical short circuit between the inner core and the outer armour. The cruise was saved by the use of a 17mm deep-tow wire on the 30-Tonne winch system for subsequent stations deeper than 4700 metres. The speed and effectiveness with which this wire was brought into use was typical of the skill and good humour shown by both scientific and ship's personnel throughout.

The authors may be contacted by e-mail at K.Heywood@uea.ac.uk, B.King@ios.ac.uk.



Figure 1. Position of CTD stations for WHP one-time cruise A23; 200 and 4000 metre isobaths are also shown.

WHP Section A3 Across 36°N Aboard RV Professor Multanovskiy

Bob Tereschenkov and Alexey Sokov, P.P. Shirshov Institute of Oceanology, Russian Academy of Sciences, Moscow, Russia; and Sergey Dobroliubov, Moscow State University, Russia

As a Russian contribution to the WHP, cruise 40 of RV Professor Multanovskiy was carried out between 11 September and 21 November 1993 (Tereschenkov *et al.*, 1994). On 15 September the ship called at Hamburg to complete a set of equipment at the Bundesamt für Seeschifffahrt und Hydrographie (BSH). In the Bay of Biscay three CTD calibration stations were occupied.

The WHP section A3 along 36°15'N took place from 23 September to 25 October 1993. The CTD survey began in the shelf break of Portugal, and ended on the shelf off North America. The cruise track and station positions are shown in Fig. 1. The section consists of 133 full-depth hydrographic stations, with a typical spacing of about 29 nm for the open ocean and around 8 nm for the stations near the ocean boundaries. Near the eastern and western boundaries the section was deviated from 36°15'N in order to cross the continental slopes perpendicular to the isobaths and to obtain a clear crossing of the Gulf Stream and the Deep Western Boundary Current (DWBC). The CTD units EG&G Neil Brown MARK-III and HYDROZOND-6000 with 24 bottles (1.7 and 1 l) were used for collecting water samples. Samples were analysed onboard for salinity, oxygen and nutrients (silicate, nitrate, nitrite and phosphate). In addition, underway measurements of meteorological data as well as near surface temperature were made.

Obtained data are compared with previously collected two sets of hydrographic data by RV Chain in 1959 and RV Atlantis-II in 1981. Considerable changes in the water mass properties at intermediate and deep layers are revealed, especially in the western part of the Atlantic (Lappo *et al.*, 1994, 1995). Fig. 2 presents the temperature differences between 1981–1959 and 1993–1981 cruises. The distribution of the temperature and salinity differences are quite the same for the same periods, but salinity changes for these periods are reverse to the temperature changes, slight freshening coincides with cooling, and slightly higher

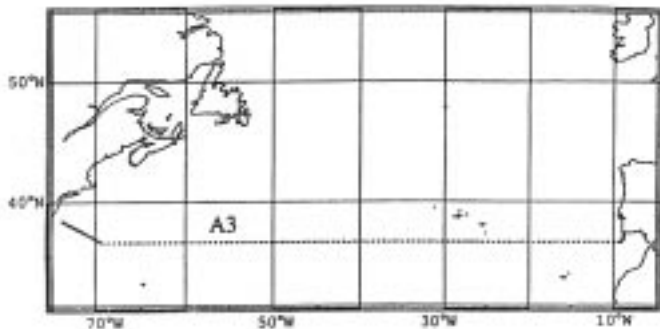


Figure 1. Station location for RV Professor Multanovskiy cruise 40.

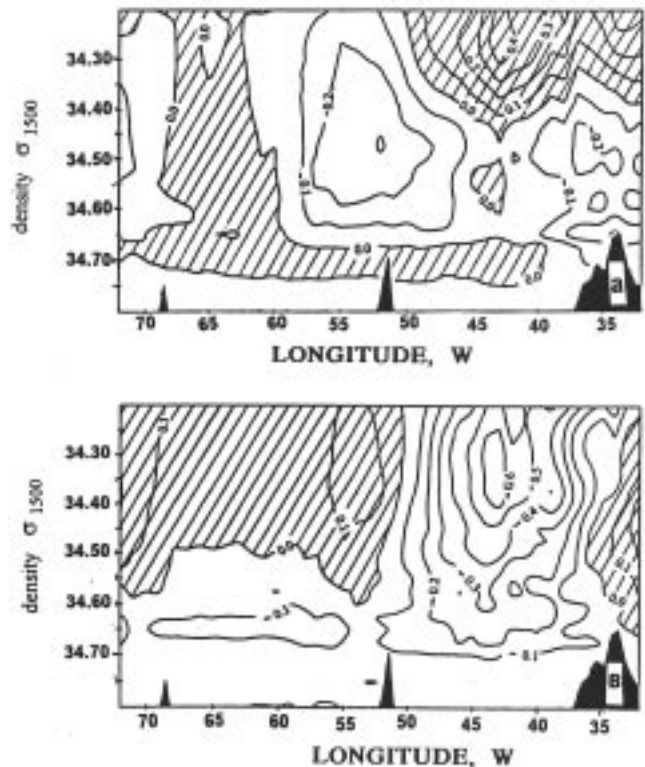


Figure 2. Temperature difference along 36°15'N: (a) 1981–1959, (b) 1993–1981. Shading indicates positive difference.

salinities are accompanied by warming.

Most conspicuous is the distinct zonal Labrador Sea Water (LSW) layer in the density interval 34.65–34.70 ($\sigma_{1.5}$) through the whole western North American Basin in which temperature and salinity differences change the sign: there was warming of LSW between 1959 and 1981 followed by cooling between 1981 and 1993. It is noticeable that the cooling and freshening in the early 1990-s are more pronounced than preceding warming and salinity increasing: -0.1 – 0.2° and -0.02 – 0.04 psu against $+0.1^\circ$ and $+0.01$ psu. Hence a general cooling and freshening took place at the intermediate depth of the western North American Basin, over the entire 34-year period. The pressure changes in LSW have a quite different tendency. The general pressure increase was found over the entire period of observations. So there is not only cooling and freshening of LSW, but it also deepened during this period.

There was no pronounced salinity minimum associated with the LSW at 36°N in 1959 and 1981. Analysis of water masses distribution (Dobroliubov *et al.*, 1995) confirms, that the cooling, freshening and deepening of the LSW, earlier registered by Read and Gould (1992) in subpolar

North Atlantic and Koltermann and Sy (1994) at 48°N, also occurred at 36°15'N in 1993. This resulted in the existence of pronounced salinity minimum of the LSW on the depths from 1800 – 2500 m throughout the whole western basin and also on a few stations just east of the Mid-Atlantic Ridge (MAR). The minimum values of salinity and temperature in the core of LSW in 1993 are 34.92–34.95 and 3.3–3.6° (Fig. 3a). The cooling and freshening of LSW in 1993 is accompanied with decreasing of oxygen deficit by 6–9 $\mu\text{mol/kg}$. But there are no changes in the nutrient concentration. That means the penetration to the south of younger LSW cores. Most conspicuous is the presence of the young LSW core with the most modified characteristics west of MAR but not in the area of DWBC.

The maximum values of the cooling and freshening (up to -0.6° and -0.14 psu) were found over the 900–1200 db layer in 5–7° temperature range west of MAR near 45°W. The tendencies of the changes in this layer between the cruises are the same but with more pronounced cooling and freshening in 1993 than in LSW. This signal is associated with the very intensive penetration of the Antarctic Intermediate Water (AAIW) to the north. In contrast to LSW the cooling and freshening in this layer is accompanied with decreasing of pressure. According to water mass distribution at 36°N in 1993 (Dobroliubov *et al.*, 1995) the salinity minimum (the main characteristic of AAIW) is well defined only near the Gulf Stream and just west of MAR. But there is a pronounced nutrient maximum associated with AAIW throughout the whole western basin in 700–1100 m depth interval and east of MAR at the same depths. The characteristics of AAIW cores at 36°N in 1993 are: σ_2 : 36.2–36.3; temperature: 7.5°–8.5°C; salinity: 34.97–35.18; nitrate up to 29 $\mu\text{mol/kg}$, silicate up to 24 $\mu\text{mol/kg}$, phosphate up to 1.7 $\mu\text{mol/kg}$, oxygen deficit 80–140 $\mu\text{mol/kg}$. There are no water masses formed in the North Atlantic with concentration of >18.13 $\mu\text{mol/kg}$ in nitrate and silicate and >1.1 $\mu\text{mol/kg}$ in phosphate. So the existence at 36°N in 1993 water with above mentioned characteristics means penetration of AAIW from the south. The cooling and freshening in the AAIW layer is accompanied by an increase of the silicate concentration by 2–5 $\mu\text{mol/kg}$, compared to 1981 (Fig. 4a). It is interesting to note that the cores of AAIW with their pronounced silicate and salinity signal now were found west of MAR. There were no clear AAIW cores observed at 36°N in 1959 and 1981. It appears to be connected with the change of the thermocline circulation in this area.

A general cooling and freshening was found in the deep layers of the western North American Basin, over the entire 34-year period. The Gibbs Fracture Zone Water (GFZW) has the following characteristics in its core in 1993: σ_2 : 36.96–36.97; temperature: 3.1–3.3°; and salinity: 34.96–34.98. If compared with 1981, GFZW became fresher by 0.005–0.01 psu. There is some increase of silicate concentration. But there are no changes in the other nutrients concentration. The Denmark Strait Overflow Water (DSOW) is also fresher in 1993 by about 0.005–0.01 psu than in 1981 (Fig. 3b). There are no changes in the

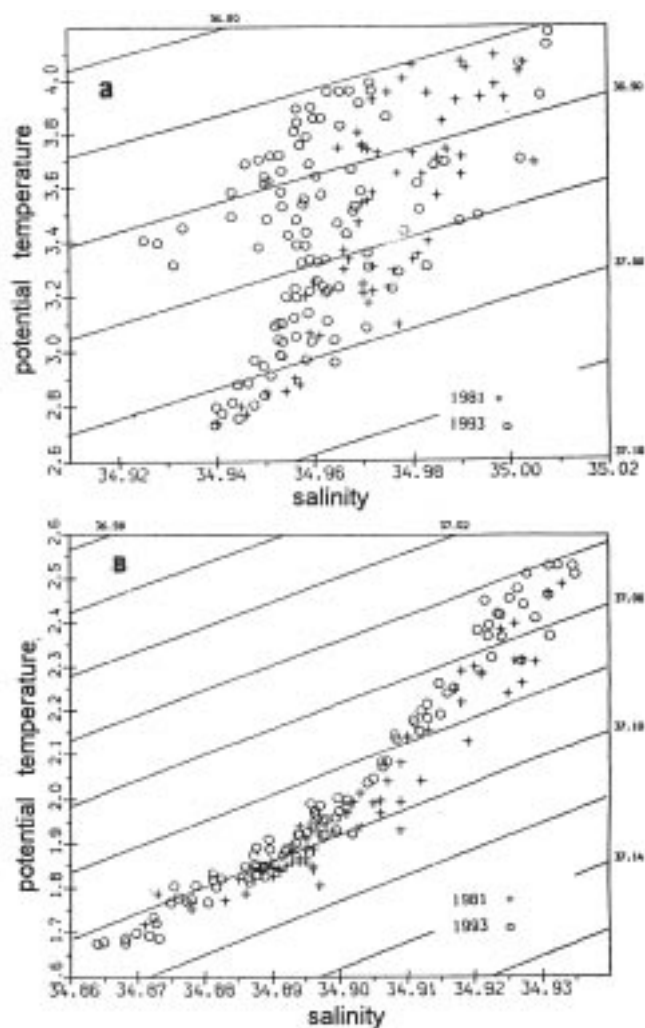


Figure 3. T-S plots of the stations from the western basin for 1981 and 1993: (a) LSW and GFZW depth interval ($\sigma_2=36.85\text{--}37.02$), (b) DSOW and AABW depth interval (σ_2 more than 37.04).

nutrients. There was also a change of properties of the Antarctic Bottom Water (AABW) near the bottom. AABW is cooler by 0.05° and fresher by 0.01 psu. There is an increase in the silicate concentration by 5–8 $\mu\text{mol/kg}$ (Fig. 4b).

There are changes in the deep water structure of the eastern basin too, but only near the bottom. There are no changes in the density interval 37.0–37.1 (σ_2). However near the bottom temperature is cooler by 0.03° , salinity decreased by 0.005 psu and the nitrate concentration increased by 2 $\mu\text{mol/kg}$. It is interesting to note that if in 1981 the silicate concentration near the bottom was higher in the western basin, in 1993 we have a reversed picture.

Thus the hydrological structure at 36°15'N in 1993 is characterised by intensive water penetration of both Antarctic and Labrador origin. The general cooling and freshening at intermediate and deep layers took place, especially in the western part of the transect. Most striking is the location of the layers with largest changes just west from MAR, away from the region of DWBC.

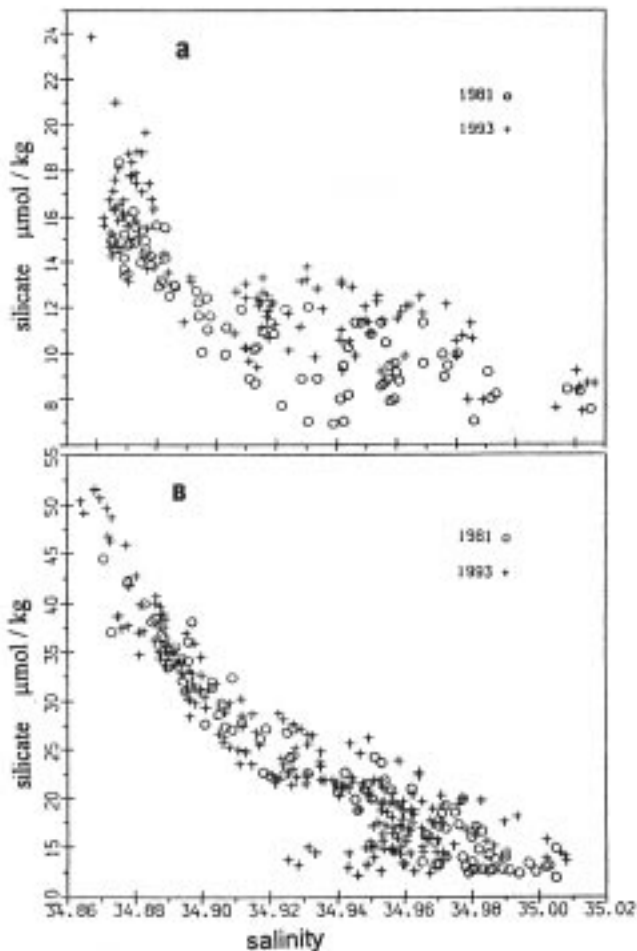


Figure 4. S-Si plots of the stations from the western basin for 1981 and 1993: (a) AAIW and Mediterranean water

Acknowledgements

The 40th cruise of RV Professor Multanovskiy was supported by the Russian Ministry of Science, the Russian Foundation of Basic Research, and BSH (Hamburg, Germany). We are grateful personally to Dr K.-P. Koltermann for his enthusiastic support of the cruise. Scientific analysis of the data was supported under the Grants ISF ME-5000, INTAS-93-2096 and "WOCE" sponsored by the Russian Ministry of Science.

References

- Dobroliubov, S.A., V.P. Tereschenkov, and A.V. Sokov, 1995: Water masses distribution on 36°N in the Atlantic Ocean in 1993. *Oceanology*, in press (in Russian).
- Koltermann, K.-P., and A. Sy, 1994: Western North Atlantic cools at intermediate depths. *International WOCE Newsletter*, No. 15, 5-6.
- Lappo, S.S., S.A. Dobroliubov, A.V. Sokov, and V.P. Tereschenkov, 1994: Long-period changes in the intermediate and deep water circulation in the North Atlantic. *ICES, C.M.1994/C:10*, 12 pp.
- Lappo, S.S., V.P. Tereschenkov, A.V. Sokov, and S.A. Dobroliubov, 1995: Freshening and cooling of intermediate and deep water in the western North Atlantic in the early 1990s. *Doklady Akademii Nauk*, in press (in Russian).
- Read J.F., and W.J. Gould, 1992: Cooling and freshening of the subpolar North Atlantic Ocean since the 1960s. *Nature*, 360, 55-57.
- Tereschenkov, V.P., S.A. Dobroliubov, and V.A. Konnov, 1994. 40 cruise of RV Professor Multanovskiy as a Russian contribution to WOCE. *Oceanology*, 34, No. 6, 934-936.

Modelling Radiocarbon Uptake by the Southern Ocean

Joachim Ribbe and Matthias Tomczak, *The Flinders University of South Australia, School of Earth Sciences, GPO Box 2100, Adelaide 5001, South Australia*

Introduction

The circulation of the Fine Resolution Antarctic Model (FRAM) is applied in the development of an off-line radiocarbon validated tracer model for the Southern Ocean. The tracer model's spatial resolution is that of the FRAM (0.5° in longitude and 0.25° in latitude and 32 levels in the vertical). It will be used to interpret the observed three dimensional distribution of radiocarbon within the Australian sector of the Southern Ocean where a radiocarbon sampling programme is being carried out along WOCE Section SR4 between Tasmania and Antarctica. Additional data come from the South Australian Basin to establish a three dimensional picture of the ¹⁴C distribution for that sector of the Southern Ocean.

This note is a brief report on the outcome of a numerical experiment which was carried out for an ideal tracer. The modelled distribution of the tracer is explained and agrees well with the known physical mechanism observed in some regions of the Southern Ocean. A notable outcome of this application is the modelled renewal of South Indian Ocean thermocline water. Surface water originating in the southeastern part of the Indian Ocean ventilates the Indian Ocean thermocline and moves northward.

Method

The equation describing transport and mixing of a scalar ocean water property is the general equation of

conservation. For a substance C, it is given (e.g. Semtner, 1986, here modified by including S) by:

$$\frac{\partial C}{\partial t} + L \cdot C = k \cdot \frac{\partial^2 C}{\partial z^2} + A_h \cdot \nabla^2 C + S$$

In this equation, L was defined as an advection operator taking the form:

$$LC = \frac{1}{a \cdot \cos \phi} \cdot \frac{\partial}{\partial \lambda} (u \cdot C) + \frac{1}{a \cdot \cos \phi} \cdot \frac{\partial}{\partial \phi} (v \cdot C \cdot \cos \phi) + \frac{\partial}{\partial z} (w \cdot C)$$

The horizontal Laplacian operator has the form of:

$$\nabla^2 C = \frac{1}{a^2 \cdot \cos^2 \phi} \cdot \frac{\partial^2 C}{\partial \lambda^2} + \frac{1}{a^2 \cdot \cos \phi} \cdot \frac{\partial C}{\partial \phi} \left(\frac{\partial C}{\partial \phi} \cos \phi \right)$$

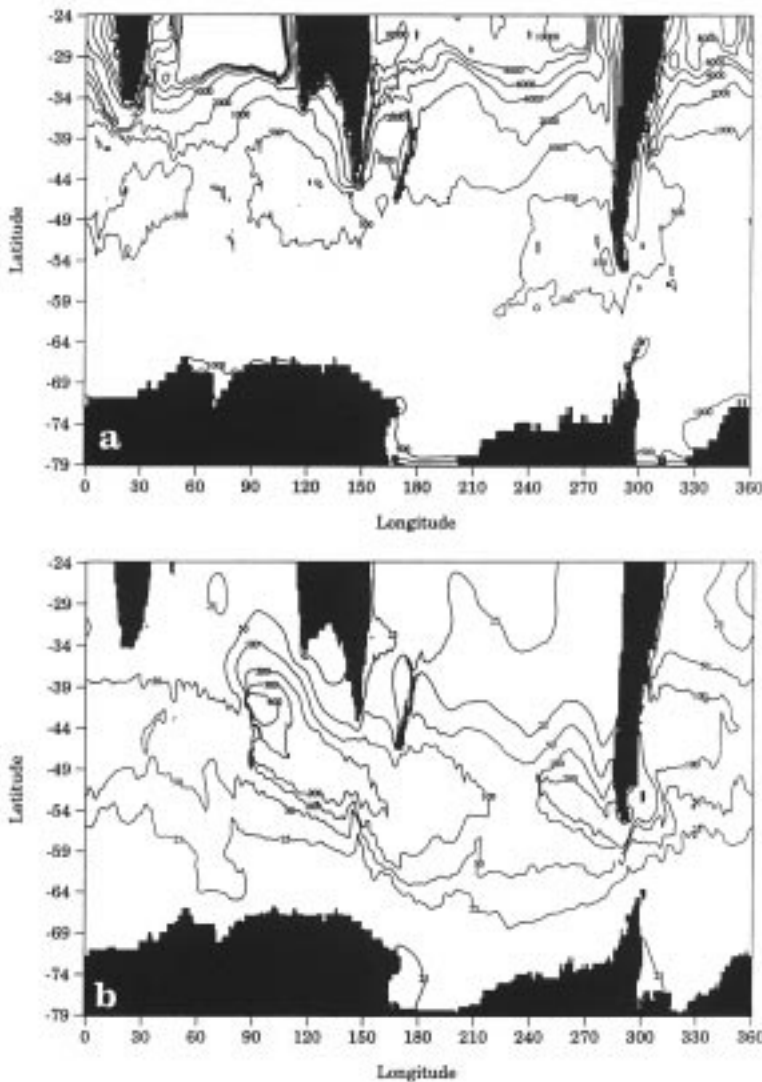


Figure 1. Distribution of the tracer in the surface layer (a), and at 290m (b) in layer 8 after five years of simulation. Contours are given in intervals of 250, 500, 1000, 2000, 4000, 6000, 8000, and 10000 (a); 25, 50, 100, 200, 300 and 400 (b).

ϕ and λ are longitude and latitude; z the vertical coordinate; a is the earth radius; k and A_h are the vertical and horizontal eddy diffusivity; t is time; u , v , and w are the components of the three dimensional velocity vector; S is a source term (including negative sources (sinks)) for C. In the case of a coarse resolution OGCM, temperature and salinity sources are usually simulated by relaxation to observed climatology. For radiocarbon, S can take a more complex form. In its simplest form, it represents radioactive decay as a sink term. In the experiment represented here, only a source term was specified. In future experiments a sink term will be introduced at the northern boundary of the model.

A copy of the vectorised form of the FRAM tracer code and other data input fields was obtained from Dr D. Stevens. The code was implemented on a CM-5 with 32 processors and 128 vector units at the South Australian Centre for Parallel Processing in Adelaide. It is possible to

increase the present computing speed further.

The initial experiments, of which an example is represented below, were carried out with the existing version of the code.

The radiocarbon-validated tracer model is being developed in a off-line version. No explicit solution is obtained for the velocity field. To solve for the unknown velocities required in the tracer equation, the results of the FRAM (e.g. FRAM Group, 1991) are applied. A mean circulation was obtained by deriving an average from the accumulated monthly data sets of year 10 to 16 of the FRAM integration. It was expected that the average velocity field would be in a steady state in a statistical sense with only a minor time-dependent fraction. Convective overturning is simulated in the tracer model by applying a convective mask derived from monthly dumps of overturning events during the FRAM integration.

Model experiments

The application of an ideal tracer allows one to study the physical mechanisms represented by the tracer model. Everywhere in this initial experiment, a tracer of magnitude '1' is introduced at the surface at each time step. The initial concentration is set to '0'. The time step is 4 hours and the model was run for a total of 5 years (i.e. 10950 time steps). In the following, the concentration in layer 1 (surface), layer 8 (290 m), and along three transects across the Southern Ocean obtained at the end of the simulation is discussed. The tracer data are represented as overlays on black and white raster images of the cross sectional velocity. Frontal zones associated with strong flow

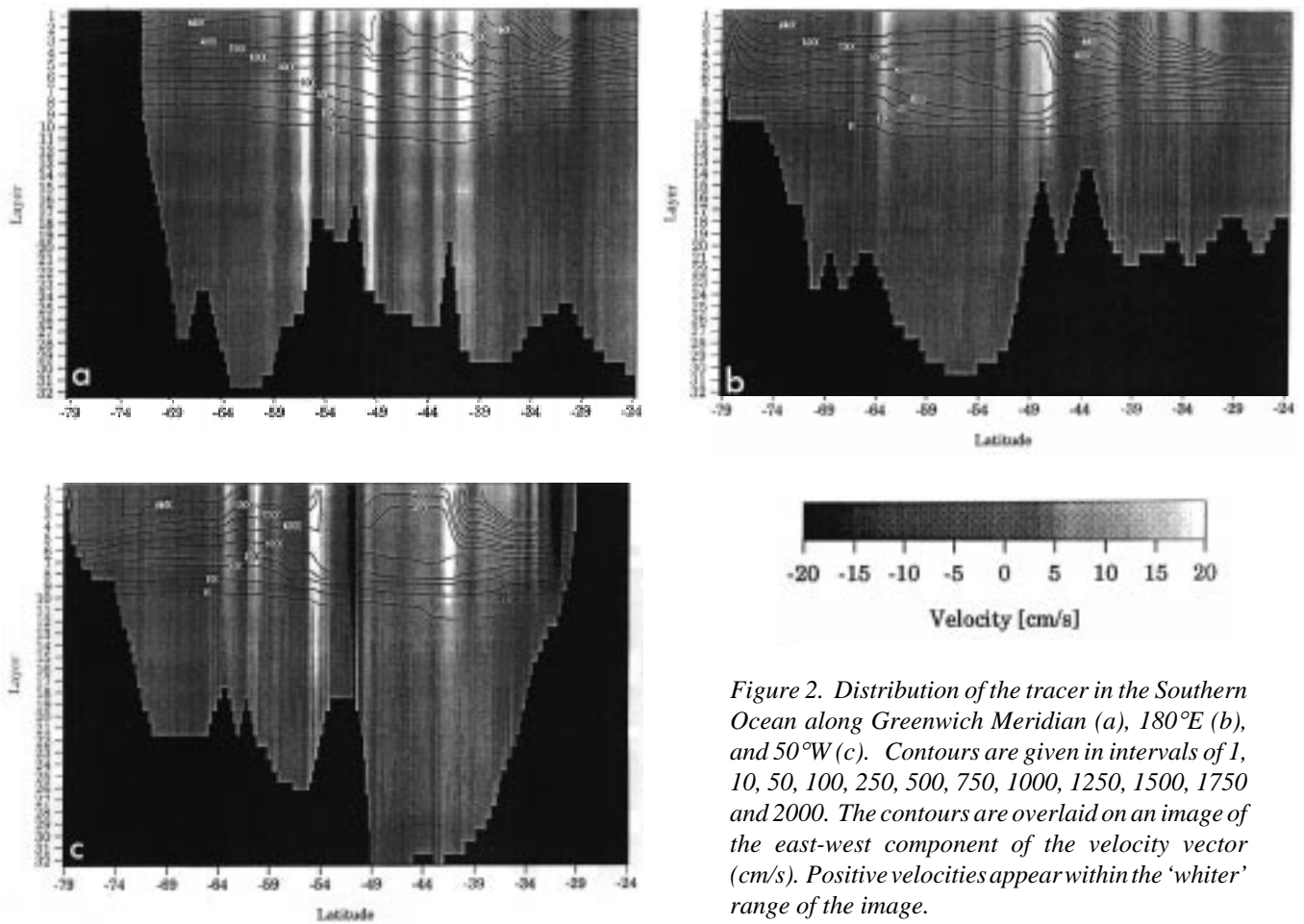


Figure 2. Distribution of the tracer in the Southern Ocean along Greenwich Meridian (a), 180°E (b), and 50°W (c). Contours are given in intervals of 1, 10, 50, 100, 250, 500, 750, 1000, 1250, 1500, 1750 and 2000. The contours are overlaid on an image of the east-west component of the velocity vector (cm/s). Positive velocities appear within the 'whiter' range of the image.

toward the east appear in white, frontal zones with strong flow toward the west appear in black.

Notice should be taken that the vertical tracer distribution occurs in layers rather than depths and therefore, a distortion of the vertical axis is shown. The thickness of the layers ranges from 20.3 m in the surface layer to 233 m in the bottom layer. The depths of layers 4, 6, 8, 10, 15, 22, 26, and 32 correspond to 86 m, 169 m, 290 m, 532 m, 1508 m, 3071 m, 3989 m and 5382 m respectively.

The concentration of the tracer in the surface layer of the Southern Ocean is represented in Fig. 1a. The large scale distribution of the tracer divides the model domain into three main regions. The highest concentration is found in the subtropical oceans. The concentration is generally lower within the path of the Antarctic Circumpolar Current (ACC) where the lowest concentration is observed in regions of deep convective overturning. Minima in the tracer concentration with values below 500 are also found in the Weddell Sea and Ross Sea. The influence of advection on the distribution is indicated in the tracer distribution. Minimal advection toward the centres of the subtropical gyres results in an accumulation and retention of the tracer while within the main path of the ACC, the tracer is advected rapidly or convected into deeper layers. Northward advection in the Tasman Sea is shown by the excursion of the 1000 and 2000 isolines. The front between

the Malvinas and Brasil currents features prominently at approximately 39°S and 55°W.

The modelled distribution in layer 8 at 290 m (Fig. 1b) represents a reversed image of the distribution at the surface. The subtropical gyres are characterised by lower concentrations, while areas of convective overturn show an increased concentration of the tracer. It is obvious, that the convection is deepest in the band between 44°S and 54°S, while close to the Antarctic continent it only reaches down to depths of 200 to 300 m. The excursion of the isolines south-west of Australia shows a north-west transport of the tracer indicating the ventilation of the Indian Ocean permanent thermocline by water subducted south of or near 39°S and 120°E. Prominent topographic features are reflected in the tracer distribution as well. The Kerguelen Plateau is indicated by the southward excursion of the isolines at around 80°E while in the proximity of the Campbell Plateau the isolines diverge.

The distribution of the tracer is determined through the interaction of advection, convection, horizontal and vertical eddy diffusivities. At the Greenwich Meridian (Fig. 2a) south of 59°S, the vertical displacement is controlled primarily by vertical diffusion. Close to the Antarctic continent and between 67°S and 70°S, a convergence is indicated by the vertical excursion of the isolines in the top 100 m of the water column. This convergence is most

likely associated with the east wind drift resulting in a southerly transport and subsequent vertical motion. The main path of the ACC is associated with a depletion of the tracer in the surface layer and an outcropping of the isoline. The Polar Front, the Sub Antarctic Front and the Subtropical Front are indicated at approximately 56°S, 50°S and 41°S respectively. The tracer is convected, or advected out of this region into the subtropical gyre. The convective displacement is indicated by the vertical excursion of the isolines between 35°S and 54°S. Further to the north of the main path of the ACC, there seems to be some indication of Ekman pumping at around 30°S down to layer 6 at 169 m.

The southern part of the transect at 180°E (Fig. 2b) is located in the Ross Sea. Convective mixing displaced the tracer down to 290 m indicated by the vertical excursion of the isolines. The northern and southern boundaries of the ACC are located at approximately 64°S and 49°S. The region in between is depleted in the top few hundred metres shown by the outcropping of the '750' isoline. The influence of topography on the flow and on the distribution of the tracer is clearly observed above the Chatman Rise at approximately 49°S. The isolines descend sharply toward the north. The highest concentration along this transect is found again in the area of the subtropical gyre where the accumulation of the tracer due to input at the surface is not opposed by strong advective or convective processes.

The other area of the Southern Ocean where known convective overturning occurs is close to the Antarctic continent is the Weddell Sea. The vertical distribution of the tracer at 50°W (Fig. 2c) is clearly influenced by the process of convective overturning down to a depth of

Neutral Density

David Jackett and Trevor McDougall, CSIRO Division of Oceanography, Hobart, Tasmania 7001, Australia

A computer algorithm is now available for labelling hydrographic data with a "density" variable, called neutral density, that is constant on neutral surfaces. This algorithm comes in the form of a FORTRAN subroutine or a MATLAB function. One cost, however, is that 2 MBytes of storage is required for an accurately pre-labelled world ocean. This ocean is essentially a very stable (in terms of N^2 profiles) version of the Levitus (1982) climatology, with some Southern Ocean topographic alterations made to ensure the labelling of Antarctic Bottom Water. A neutral density field has been optimally generated, in the sense of satisfying the underlying neutral density equations, for this stable ocean. By neutral density equations we mean the differential equations which define the gradient of the locally referenced potential density $\rho(\beta\nabla\theta - \alpha\nabla S)$ as being in the direction orthogonal to the neutral surfaces. Neutral surfaces are those surfaces having the property that small adiabatic and isentropic displacements of fluid parcels in the surface do not produce restoring buoyancy forces on the parcels. Data from the real world quadratically interpolates this neutral density field.

290 m (layer 8). The main path of the ACC is observed between 63°S and 41°S with the most distinct front, *i.e.* the highest horizontal velocities, located at 53°S. North of 54°S convective mixing also results in a vertical excursion of the isolines while between 44°S and 39°S some influence of Malvinas-Brasil confluence is observed in the vertical tracer distribution.

Conclusion

The observed distribution of an ideal tracer seems to agree well with the known physical processes operating within the upper 1000 m the Southern Ocean. To investigate the model's performance in the deep layers a longer integration of the model is required. For the study of the distribution of radiocarbon in the Southern Ocean, however, this model is appropriate.

Acknowledgement

We would like to thank Dr D. Stevens for providing the FRAM tracer code and data input fields.

References

- FRAM Group, 1991: An eddy-resolving model of the Southern Ocean. *Eos. Transaction. AGU.* 72(15), 174–175.
- Semtner, A.J., 1986: Finite difference formulation of a world ocean model. In: *Advanced Physical Oceanographic Modelling.* J.J. O'Brien (ed.). 187–202.

The necessity for the ocean atlas arises from the fact that neutral density is not a well defined function of the three state variables S , θ and p . This fact has been known for some time, *e.g.*, Lynn and Reid (1968) realised that water masses on the same "isopycnal" emerge with significantly different σ_θ values in the two hemispheres. The present best method of defining neutral surfaces appears in Reid (1994), where neutral surfaces are approximated by a linked sequence of potential density surfaces referred to a discrete set of reference pressures. Reid has defined 10 surfaces in the North and South Atlantic Oceans by some 88 parameters, within 11 distinct regions, using 8 different reference pressure levels. These parameters and reference levels are related as one changes regions. Additional or different surfaces require more parameters, and perhaps more regions and reference pressures, which all require matching. Neutral density, γ^n , which is the continuous analogue of these discrete Reid surfaces, is a continuous function of $\{S, \theta, p, \text{longitude, latitude}\}$, and as such is extremely easy to use.

In the strict mathematical sense, neutral surfaces do

not exist. However, our neutral density variable is a well defined function of $\{S, \theta, p, \text{longitude, latitude}\}$, implying we have sacrificed the exact neutrality of our variable in order to have it well defined. The ill-defined nature of neutral surfaces arises from the non-linear terms in the equation of state of seawater, in particular, from the dependence of the thermal expansion coefficient on pressure. However the ambiguity in accurate global neutral excursions is so small, being of $O(10 \text{ metres})$, that the errors incurred in properly defining a well defined five dimensional variable are below the present instrument error of 0.005 kg m^{-3} .

The global data set was labelled with neutral density in the following manner. The world ocean provides a domain within which we can solve a system of first order hyperbolic partial differential equations (pde's), these being the statement of the neutral density property in this domain. At each location we have two independent pde's describing the one property γ^n , so the resulting system of equations is overdetermined. These equations have been solved using a combination of techniques; the method of characteristics in nearly 85% of the ocean and finite

differences in the remaining 15%. This solution has been further iterated in the problem's natural characteristic coordinate system, providing a γ^n field whose errors from all sources, including the inherent helical errors, are on average an order of magnitude less than current instrument error. Complete details on how the Levitus ocean is modified and how the pde system solved can be found in Jackett and McDougall (1995).

The global data set actually limits the extent of $\{S, \theta, p, \text{longitude, latitude}\}$ space for which γ^n is defined. In this data set we have excluded the Arctic Ocean, the Mediterranean, Baltic, Black, Caspian and Red Seas, the Persian Gulf and Hudson's Bay. Otherwise, we have a regular $4^\circ \times 4^\circ$ grid of stable Levitus data, with minor modifications in the Antarctic region, along with an estimate of its γ^n field. We also provide error estimates of the γ^n values in the form of two error bars $\{d\gamma_l^n, d\gamma_u^n\}$. Over most of the ocean these error bars are small and equal, however in Antarctic waters $d\gamma_u^n$ exceeds $d\gamma_l^n$ to account for the sinking of Antarctic Bottom water from the shelf to great depth.

The user has a bottle $\{S, \theta, p, \text{longitude, latitude}\}$, or more usually a cast $\{(S_k, T_k, p_k, \text{longitude, latitude}), k = 1, 2, \dots, n\}$ requiring labelling with γ^n . The language implementation is essentially a function *gamma_n* with output parameters $\{\gamma_k^n, \gamma_l^n, \gamma_u^n, k = 1, 2, \dots, n\}$. Internally the code interpolates the labelled data set by taking a weighted average of the (up to) four closest casts from the labelled data set. The interpolation error incurred in this calculation is one possible source of error contained in the error bars $\{d\gamma_l^n, d\gamma_u^n\}$. Other errors are the natural helical errors in the labelled data set and the errors from possible Antarctic Bottom Water formation.

We have also provided another function *neutral_surfaces* which, given a cast of labelled data $\{(S_k, T_k, p_k, \gamma_k^n, k = 1, 2, \dots, n)$ and γ^n surfaces $\{\text{gsurface}_i, i = 1, 2, \dots, \text{ns}\}$ returns the positions of the specified γ^n surfaces, together with error bars $\{(\text{sns}_i, \text{tns}_i, \text{pns}_i, \text{dsns}_i, \text{dtns}_i, \text{dpns}_i), i = 1, 2, \dots, \text{ns}\}$. The method of interpolation is quadratic, building in the non-linearity of the equation of state. The error bars are usually zero, but when they are non-zero they represent inversions in the data, which are almost certainly due to buoyancy frequency problems (*i.e.*, $N^2 < 0$) in the user's data.

In order to demonstrate the effectiveness of neutral density in accurately representing neutral surfaces in the real ocean, we have sampled the Reid global data set (*e.g.*, Reid 1994) to obtain sections of hydrographic data which are completely independent of the global data set underlying the definition of γ^n . Since the Reid data set is scattered in spatial location, we have chosen sections to be as close as possible to a particular meridian of longitude, with a zonal resolution of about 4° of latitude. We have taken such sections in the Atlantic Ocean along which we compare neutral surfaces obtained by vertically interpolating γ^n , using the *neutral_surfaces* code, with surfaces calculated using

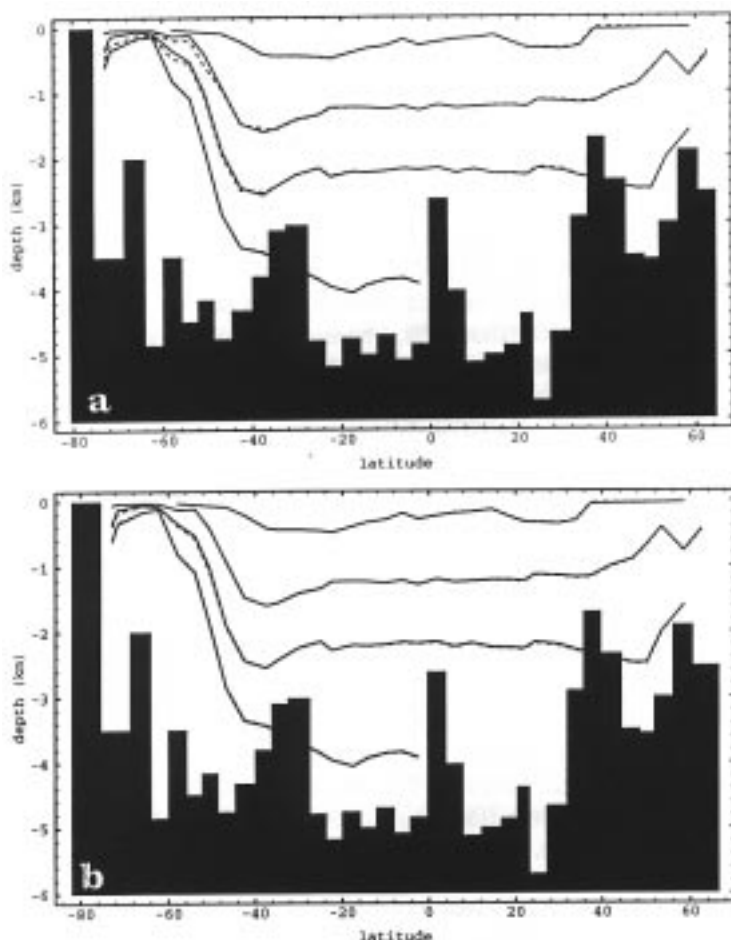


Figure 1. A meridional section in the Atlantic Ocean along approximately 330°E taken from the Reid global data set. (a) Dashed lines: first, third, fifth and ninth "isopycnal" surfaces defined in Reid (1994); solid lines: closest γ^n surfaces corresponding to these isopycnals. (b) Solid lines: γ^n surfaces of (a); dashed lines: neutral surfaces generated using an accurate neutral surface calculation, emanating from a point near 20°S .

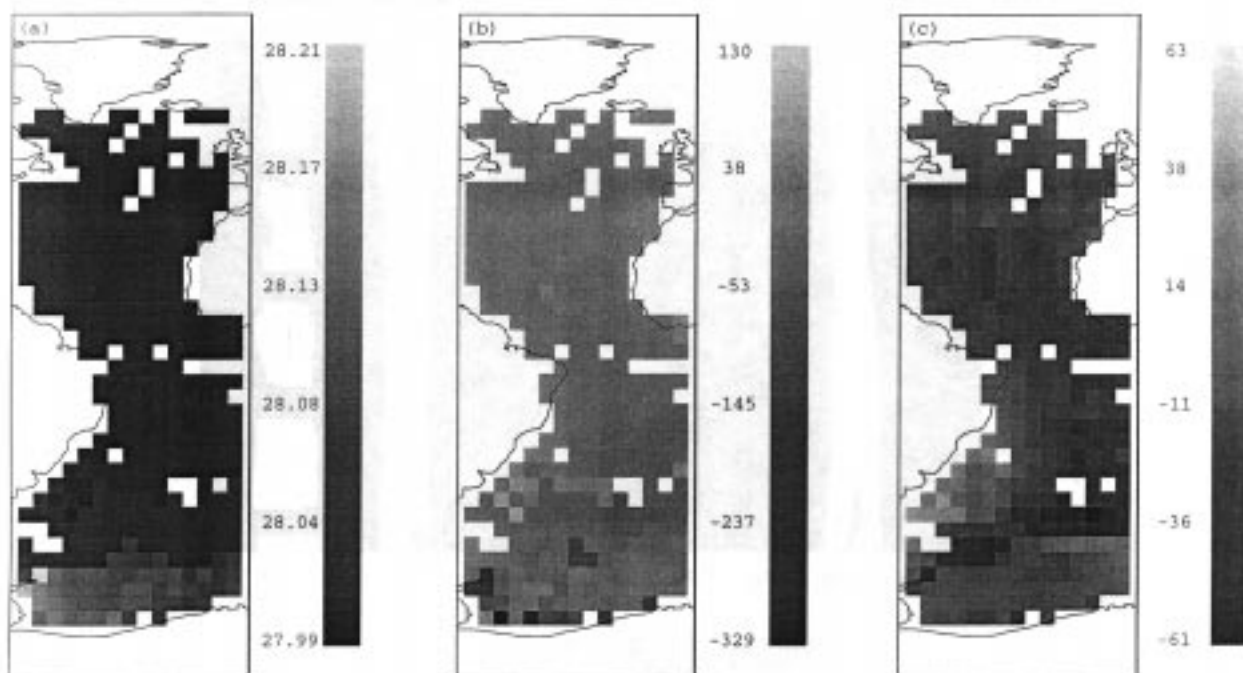


Figure 2. Plots of the fifth isopycnal from Reid (1994) in the North Atlantic Ocean. The distribution of γ^n on this isopycnal is shown in (a), whilst (b) shows the differences in depth between this isopycnal and a “best fit” γ^n surface to this isopycnal. Panel (c) plots the differences in depth between this “best fit” γ^n surface and a neutral surface generated using an accurate neutral surface calculation, emanating from a coincident point in the central Atlantic. The differences in the depth scales between (b) and (c) indicate the improvement made by using γ^n surfaces over the isopycnal surfaces of Reid (1994) in approximating neutral surfaces.

several alternative methods, including the afore-mentioned present best “isopycnal” surfaces.

Fig. 1a shows the first, third, fifth and ninth isopycnal surfaces of Reid (1994), based on potential density surfaces with a discretely varying reference pressure, on a meridional section near 330°E in the Atlantic Ocean. These surfaces are depicted by the dashed lines, with the corresponding γ^n surfaces (solid lines) being defined as those γ^n neutral surfaces which minimise the mean absolute deviations (in terms of depth) from the corresponding Reid isopycnals. In general, these “isopycnal” surfaces, although cumbersome to calculate, approximate the neutral surfaces well, although in southern regions they can differ by nearly 200 metres. The mean absolute deviation between the two sets of surfaces is 15.4 metres with the maximum absolute deviation being 179.8 metres. This section was typical of all the meridional sections in the Atlantic Ocean. In Fig. 1b we show the neutral surfaces defined using a very accurate basic neutral surface calculation (dashed lines) for the same four γ^n surfaces of Fig. 1a (solid lines, formed using the neutral surfaces code) in the Atlantic. This accurate calculation is expensive to perform, and has the added disadvantage of being completely independent of a label (see Jackett and McDougall (1995) for a description of this accurate neutral surface calculation). In this case the mean absolute differences in depth between the two sets of surfaces is 7.7 metres whilst the maximum absolute deviation is 50.9 metres. This latter figure demonstrates the accuracy of the γ^n surfaces in approximating the fundamental neutral surface property.

In Fig. 2 we have concentrated on one particular “isopycnal” surface of Reid (1994), namely his fifth surface (the third surface in Figs. 1a and b). Fig. 2a shows the variation of γ^n on this isopycnal over the Atlantic Ocean between 300°E and 0°E, where a variation of 0.22 kg m⁻³ in γ^n is evident. In Fig. 2b we show a map of the differences in depth between the “best fit” γ^n surface and this particular isopycnal. By “best fit” we again mean that γ^n surface which minimises the mean absolute depth deviation from the Reid isopycnal. The mean absolute deviation of this γ^n neutral surface (where $\gamma^n = 28.0092$) from the Reid isopycnal is 28.4 metres over the region shown, with a maximum absolute deviation in the Weddell Sea of 328.8 metres. To test which of these surfaces is the more accurate in approximating the neutral surface property, we have compared this $\gamma^n = 28.0092$ neutral surface with a neutral surface computed using an accurate method of generating neutral surfaces in two lateral directions (see Jackett and McDougall (1995)). The surface was chosen to emanate from the central location of (324°E, 10°S) at the depth of the γ^n surface. Fig. 2c shows the differences in depth between these two distinct neutral surfaces, the mean and maximum absolute differences being 11.8 metres and 63.3 metres respectively. The small sizes of these two errors, compared with the magnitudes of the same errors associated with Fig. 2b, again indicate the increased accuracy of using γ^n surfaces in approximating neutral surfaces over the present best isopycnal surfaces of Reid (1994).

While our γ^n surface more accurately approximates a neutral surface than does the best-practice isopycnal

approach of Reid (1994), the improvement may well not be important for many oceanographic studies. Rather, we believe that our γ^n algorithm gives oceanographers a way of forming neutral surfaces much more easily than is presently available by the isopycnal method of Reid. The extra accuracy is an added bonus. Also, at the present time these Reid isopycnal surfaces have only been defined for the North and South Atlantic and South Pacific Oceans. The γ^n surfaces are, on the other hand, defined for the entire extent of the ocean excluding the Arctic Ocean and the enclosed marginal seas.

The neutral density code can be accessed through the World Wide Web at <http://www.ml.csiro.au/~jackett/NeutralDensity>.

New Depth Equation for 'Old' Sparton XBT-7 Expendable Bathythermographs

P. Rual, Surtropac Group, ORSTOM, Noumea, New Caledonia; A. Dessier and J.P. Rebert, ORSTOM, Brest, France.

New depth-time equation

The probes evaluated here are the old 'first generation' XBT-7 (760 m) manufactured by Sparton of Canada until 1992.

All XBT data are evaluated relative to a field standard, the conductivity-temperature-depth (CTD) profiler. In early 1993, during the A7 WOCE cruise, 27 'Old' Sparton XBT-7 probes were compared to simultaneous CTD profiles in the tropical Atlantic (see Fig. 1), of which two had to be eliminated for various reasons.

For the XBT-7, the depth-time equation provided by Sparton is identical to the Sippican/Tsurumi-Seiki (TSK) equation for T-4, T-6 and T-7 probe types:

$$z_m = 6.472 t - 0.00216 t^2 \quad [1]$$

where z_m is the depth and t is the elapsed time, in seconds, starting when the probe hits the surface.

Following the method described in International WOCE Newsletter No. 17 (1994) the new depth-time equation for the 'Old' Sparton XBT-7, at a confidence level of 95%, becomes:

$$Z = (6.624 \pm 0.046) t - (1.96 \pm 0.40) 10^{-3} t^2 \quad [2]$$

Observed variability and the manufacturer's specifications

Fig. 2a shows the distributions, for the 25 XBT-7 profiles, of the 681 detected depth-errors (using equation 1), as a function of their CTD depth. The data are generally outside the manufacturer's specifications (± 5 m or $\pm 2\%$ whichever is the greatest), except close to the surface where the mean depth-error is within 15 m down to a depth of 200 m. The mean depth-error ranges from zero at 100 metres to -20 m at 700 m. Only the very slow fall rates,

References

- Jackett, D.R., and T.J. McDougall, 1995: A neutral density variable for the world's oceans. Submitted to *J. Phys. Oceanogr.*
- Levitus, S., 1982: *Climatological Atlas of the World Ocean*, National Oceanic and Atmospheric Administration, U.S. Department of Commerce, Prof. Paper 13, 173 pp.
- Lynn, R.J., and J.L. Reid, 1968: Characteristics and circulation of deep and abyssal waters. *Deep-Sea Res.*, 15, 577-598.
- Reid, J.L., 1994: On the total geostrophic circulation of the North Atlantic Ocean: flow patterns, tracers and transports. *Progr. in Oceanogr.*, 33, 1-92.

outside minus one standard deviation, are entirely within the specifications down to the maximum depth.

When equation 2 is used (Fig. 2b), the mean depth-error is greatly reduced and is now within 12 m of the CTD depth. However, even the 2-standard deviation confidence interval is not entirely within the specifications. A linear approximation of the 2 and 3 standard deviation curves (dotted lines in Fig. 2b) gives respectively:

$$\pm(5m + 0.8\% \text{ of the depth}) \quad [3]$$

$$\pm(7.5 m + 1.0\% \text{ of the depth}) \quad [4]$$

The mean depth-error curve in Fig. 2a is not far from linear, thus only a linear correction approximation will be presented here to correct z_m calculated using equation 1. In order to minimise the absolute depth-error while keeping the relative one within reasonable bounds in the first hundred metres (see UNESCO, 1994), the best linear approximation (Z_1) adopted for correcting the depth is:

$$Z_1 = 1.027 z_m \quad [5]$$

The maximum errors induced by using this linear coefficient, instead of the exact correction equation, are +0.5 m and -1.5 m for the absolute error, whilst the relative depth-error is in the range +0.2% to -0.4%.

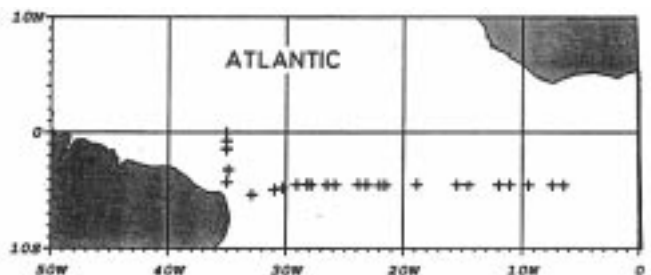


Figure 1. Locations where the 25 valid CTD/'Old' Sparton XBT-7 comparison experiments were conducted.

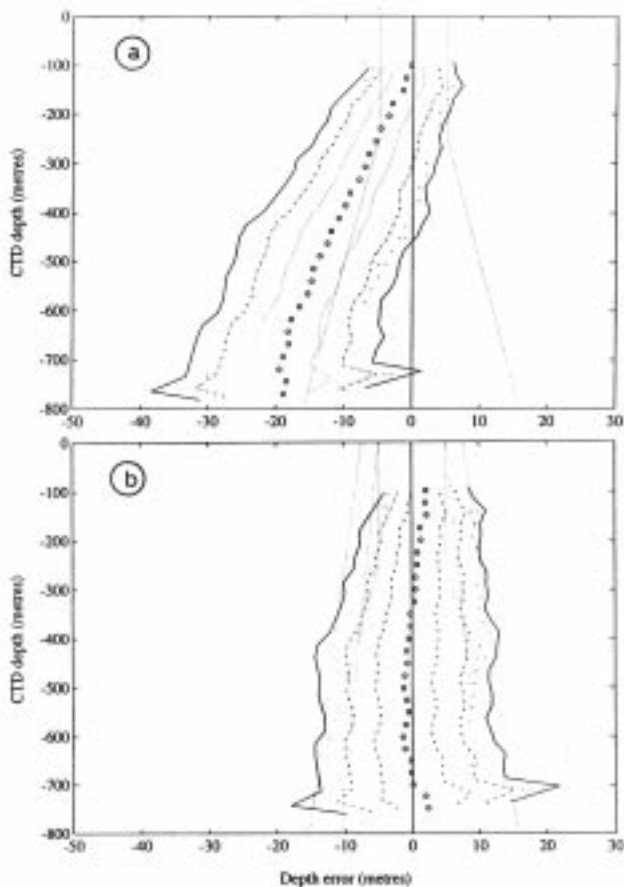


Figure 2. 'Old' Sparton XBT-7 data set: depth-errors and their statistics as a function of depth. (a, top) Using the manufacturer's depth-time equation 1. Mean depth-error (open circles) and the 1, 2, 3 standard deviations curves (respectively dotted, dash-dotted and full curves). The individual depth-errors above 2 standard deviations are also added (dots). The manufacturer's specifications (± 5 m or $\pm 2\%$ of the depth, whichever is the greater) are indicated as dotted lines. (b, bottom) Same figure, but using the new Sparton XBT-7 equation 2. Linear approximations of the 2 and 3 standard deviation curves are also

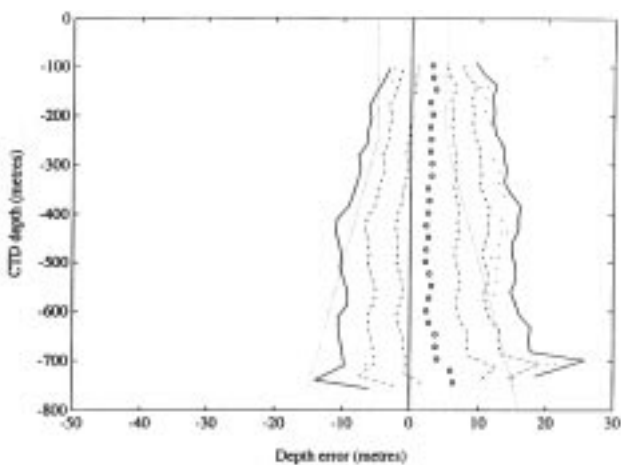


Figure 3. 'Old' Sparton XBT-7 data set: same as Fig. 2a, but using the Sippican/TSK T-4, T-6, T-7 depth-time equation

Comparing Sippican/TSK T-4, T-6 and T-7 probes with the new reference equation

In UNESCO (1994), or in Hanawa *et al.* (1994), is given the following new reference equation for the Sippican/TSK T-4, T-6 and T-7 probes:

$$Z = (6.691 \pm 0.021) t - (2.25 \pm 0.30) 10^{-3} t^2 \quad [6]$$

The statistical ellipses (not shown) of the time coefficients of the two equations do not intersect, meaning that these equations are statistically different at a confidence level of 95%. But the mean-depth-error induced by using equation 6 for the 'Old' Sparton XBT-7 probes is only +3 m down to 600 metres and increases up to +6 m at 750 metres (Fig. 3). These results imply that equation 6 can also replace the manufacturer's equation 1.

It should be stressed that the scatter of the Sparton probes is notably smaller than that of the Sippican/TSK probes (7.5 m+1% of the depth [4], instead of 9 m+2% of the depth, for the 3-standard deviation curves, see Hanawa *et al.*, 1994). But this could be due to the fact that only three boxes of a single Sparton probe-type were launched in a single area, by one institution using a single digital onboard unit, whilst the Sippican/TSK probes were of three probe types, collected in many areas by several institutions and recorded using many types of digital onboard units. In fact, individual Sippican T-7 data sets in this previous study had a very similar scatter (see Table 1a in UNESCO, 1994).

Discussion and recommendations

A new fall rate equation for the 'Old' Sparton XBT-7 was conclusively determined. The variability of the probes' characteristics was found comparable to the variability of similar Sippican/TSK probes. An acceptable error is induced when replacing that new equation by the new reference equation proposed for the Sippican/TSK T-4, T-6 and T-7 probes by Hanawa *et al.* (1994), meaning that this last equation could be used for the Sparton XBT-7 as well as for Sippican/TSK probes.

It should be noted however that the 'New' XBT-7 probes, manufactured by Sparton of Canada since 1992, will also need careful independent evaluation. To avoid any inconsistencies, it is strongly recommended that, until an international mechanism is established to implement general use of new equations, the original manufacturer's equation, only, is used for any exchange of data.

References

- Hanawa, K., P. Rual, R. Bailey, A. Sy, and M. Szabados, 1994: A new depth-time equation for Sippican or TSK T-7, T-6 and T-4 expendable bathythermographs (XBT). (Accepted by Deep-Sea Res.)
- UNESCO, 1994: Calculation of new depth equations for expendable bathythermographs using a temperature-error-free method (application to Sippican/TSK T-7, T-6 and T-4 XBTs). UNESCO Technical Papers in Marine Sciences, 67, in press.

Locating WOCE Data on the Internet

N.P. Holliday, WOCE IPO

WOCE operates a distributed data management system; data are assembled and quality controlled at Data Assembly Centres (DACs) and some are sent to Special Analysis Centres (SACs) where derived datasets and products are generated. All DACs and SACs can now be accessed via the World Wide Web (WWW), and the WOCE Data Information Unit (DIU) is the best place to start exploring the WOCE data system. The DIU homepage gives an overview of the entire data management system and provides hyperlinks to all the DACs and SACs, plus a series of related data sources such as model output and satellite data.

Newcomers to the World Wide Web

Even if you are not a seasoned “surfer” of the Web and don’t know your URLs from your HTMLs, WOCE data are still within your reach on the WWW. Browsing software is available *free* at various anonymous ftp sites, and widely used packages are Mosaic (<ftp.ncsa.uiuc.edu>) and Netscape (<ftp.netscape.com>). Demonstrations and help on how to get started come with these software. Both packages may be available at an alternative ftp site near to your work location; for more information e-mail mosaic@ncsa.uiuc.edu or info@netscape.com.

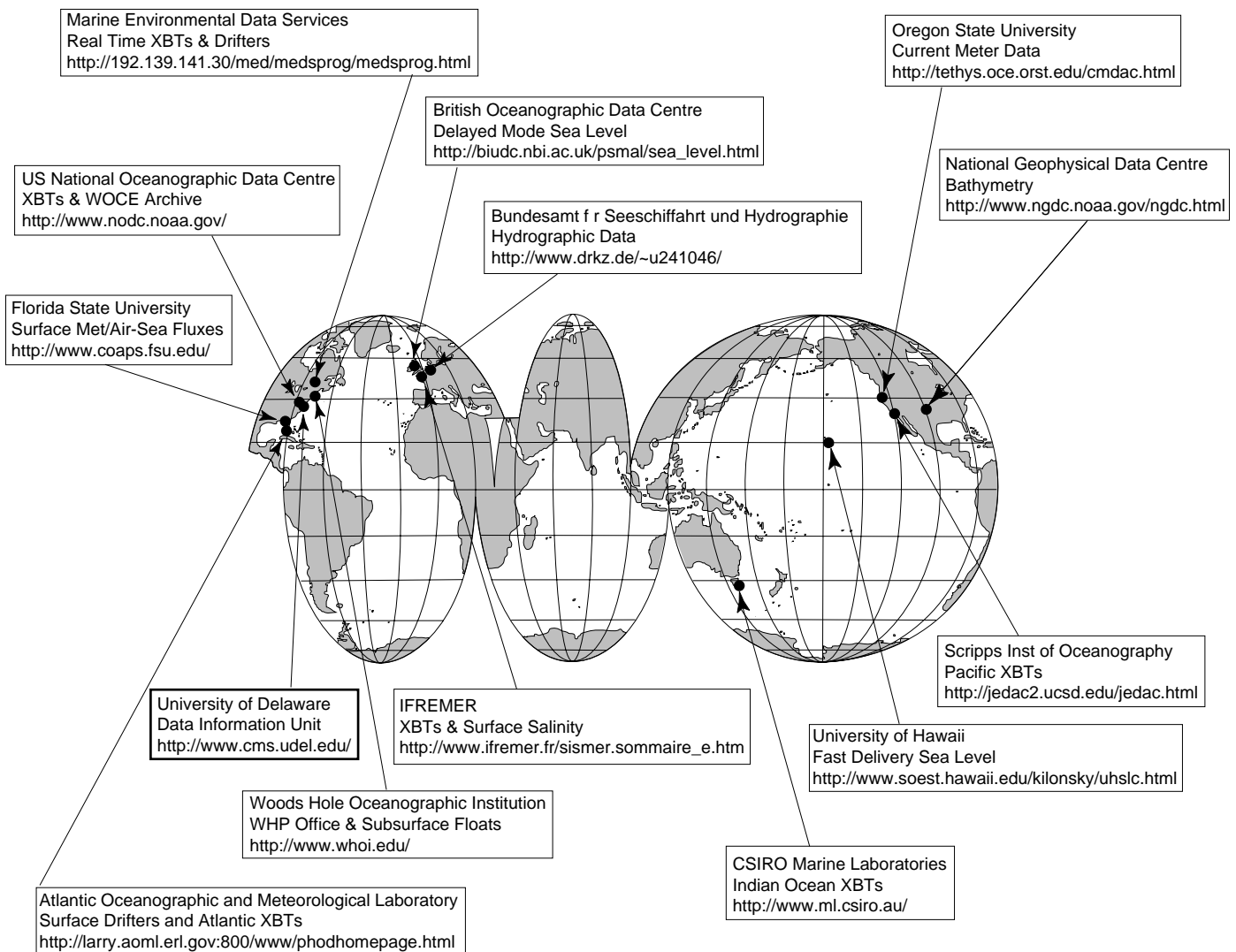


Figure 1. WOCE Data Assembly Centres and Special Analysis Centres

Rapid Dissemination of WOCE Science Results

Peter Saunders, WOCE IPO

The interval between the submission of a scientific paper to a refereed journal and its publication is seldom less than six months and frequently as long as two years. During this time copies of the manuscript are circulated to friends of the author and then to their friends and often too to students. In the belief that the rapid dissemination of the results of WOCE science must benefit both the programme and oceanography generally, we wish to systematise this dissemination process, and to make research work more rapidly and more widely available. Accordingly the following scheme is proposed.

When you submit a manuscript to a journal for review lodge an electronic version of the ABSTRACT on a local ftp anonymous server or WWW server and then advise the DIU of its location. After confirming its completeness, the DIU will add it to a list of such WOCE abstracts. Anyone who accesses the list via WWW software (*e.g.* Mosaic) can then reach an item that they select, read the abstract and be made aware of new research.

The concept/practice suggested is as follows:

- The author retains possession of his abstract, and can withdraw or modify it at a moments notice (no copy is kept at the DIU).
- The periodical targeted for publication is identified.
- The status of the manuscript (*e.g.* submitted, accepted, in course of printing) is to be attached and updated as appropriate.
- When the manuscript is published the item is withdrawn from the list and should shortly then appear in the companion WOCE bibliography.
- The copyright status of the article from which the abstract is drawn should be stated, in order to protect author, journal and the DIU.

The practical steps to be followed are as follows:

- (1) Create a plain text file of the title, affiliation, targeted journal, status (including copyright) and abstract. Also add the completion date of the manuscript. Please add your email address for correspondence.

Note the file created MUST have line breaks.

- (2) Edit the file removing all Greek symbols, umlauts, degree symbols and other non ASCII characters.
- (3) Lodge the file you have created in a directory of an anonymous ftp server or a webserver.
- (4) Please view your document either through an ftp command (ftp server) or a full Mosaic URL entry (webserver). Then advise the DIU of the correct address, the title of the manuscript and the name of your 'abstract file'. The DIU email address is:
diu@cms.udel.edu
- (5) If instead of a plain text file you wish to produce a HTML file, which will appear as a formatted page when viewed in Mosaic, add the appropriate control characters at step 2. This step is optional. (There are a number of ways to learn about HTML, the HyperText Markup Language used by the WWW. A simple way, for example, is via "A beginners guide to HTML" (<http://www.ncsa.uiuc.edu/General/Internet/WWW/HTMLPrimer.html>).
- (6) Follow steps 3 and 4 above.

We believe that the work involved to an individual scientist is quite small and that most will be willing to undertake the effort (especially after the first). For those for whom the archiving of an entire manuscript in electronic form is attractive we would draw attention to the service offered by Stephen Griffies at GFDL, Princeton for general oceanographic results (<http://www.gfdl.gov/~smg/pointers/announcement.html>). Along slightly different lines Dennis Boccippio at MIT has established a electronic collection of data and material supplementary to (published) oceanographic and meteorological texts. The address is http://www-cmpo.mit.edu/met_links/index.html.

Both of these sites offer something much more comprehensive than is proposed here. Here we offer a scheme for sharing WOCE abstracts – but of course this does not exclude those who utilise HTML adding the links to the full text and figures at their own or other sites if they so wish.

WOCE Bibliography

An important end-product of WOCE is scientific publications. A joint project, funded by Canada, between the WOCE IPO, the DIU and the UK National Oceanographic Library, has, over the past year, produced a bibliography of WOCE publications since 1983. The early phases obviously produced lots of papers and articles about WOCE planning but there are numerous important results already reaching the journals. (It would help the compilers of the bibliography if the word WOCE appeared explicitly in the abstract.) At present we have 1100 entries and we will shortly be giving each country our present list of their WOCE publications so that errors and omissions can be rectified.

The bibliography is available on line under the heading "Bibliography" on the WOCE DIU WWW Home page or directly via the URL at

http://diu.cms.udel.edu/woce/woce_bib.html

The bibliography can be searched on keywords, countries and authors. We encourage you to explore it and hope you will find it useful. Please send any comments you may have on to the IPO and/or DIU.

The Global Ocean Observing System (GOOS)

Nicholas Flemming, IOSDL, Brook Road., Wormley, Godalming, Surrey GU8 5UB, UK

The objective of GOOS is to combine the scientific knowledge of the ocean with modern technology to design and implement a continuous and routine operational oceanographic observing system which will transmit data to modelling centres, and generate useful products. These products can range on a timescale from 10 days up to 10 years.

The concept of GOOS is easy to envisage but difficult to achieve in practice. Only 10 years ago it would have seemed a pure dream. But global ocean experiments like TOGA, WOCE, JGOFS, LOICZ, and GLOBEC have improved the knowledge of the ocean-atmosphere system. Advanced coupled numerical models, ocean data acquisition by remote sensing and the increase in computing power lead to conditions which make GOOS now conceivable and possible.

The relationship between GOOS and existing major scientific oceanographic programmes has been much debated. The design of GOOS must be based on the outcome of these science experiments. They are essential precursors to GOOS. Furthermore, in the developmental stages of GOOS the large data sets acquired by these experiments will constitute an important part of the total data available, even if it is not in real time or near real time. As each ocean variable or parameter becomes sufficiently understood to be measured and processed in an automatic and routine manner, so that component can be added to GOOS after appropriate trials and tests. We can see at once that some variables are already sufficiently mature to be handled in an operational manner, while others, no less important, still require research and development. Factors which are almost ready to go globally operational, or are already assimilated on a routine basis into models, include surface wind stress, wave spectra, sea surface temperature, and dynamic topography of the ocean surface. Over certain regions XBT, CTD, ADCP, surface drifting buoys, subsurface drifters, and sea ice data are routinely measured and assimilated into predictive models.

The Ocean Observing System Development Panel (OOSDP), has completed its final report and recommendations on the scientific design requirements for the Climate Module of GOOS, which is also the Ocean component of the Global Climate Observing System (GCOS). The report identifies several variables, such as CO₂, carbon budget, or phytoplankton concentration, which are important for climate modelling, but for which it is not yet possible to obtain routine global data sets.

GOOS will provide benefits in the areas of management of coastal and shelf seas, monitoring the health of the ocean, climate variability and change, management of living resources, and operational services. The elegance of

the design of GOOS is in the assumption that it is possible to specify, for example, a sea surface temperature sampling and modelling strategy, which will meet all the user requirements, without unnecessary duplication. The design would naturally include different models, nested and interfaced on differing scales, including different variables, and with different resolutions and time scales. At every stage of the design, those scientific criteria which have been well tested will, if possible, be included.

Once a substantial range of variables are incorporated into the operational system, there will be a constant need for scientific input. It is likely that there will be a steady series of sensitivity trials in which the existing system will be examined and tested in comparison with a range of modifications, improvements, or simplifications.

WOCE now moves into its phase of analysis, interpretation, modelling and synthesis based on the completion of the seagoing observations. It is important to consider the possible elements of continuity which will support the implementation of GOOS. This might include continuing some elements of WOCE within CLIVAR, or the identification of WOCE scientific observations which might be continued with operational rather than science budget funding. Above all, the experience and knowledge gained from WOCE must be used to identify the minimum critical routine observations needed to monitor ocean circulation. Many of these implications in respect of climate monitoring are included in the OOSDP Report.

GOOS evolved from a series of decisions, resolutions, and agreements within and between the Intergovernmental Oceanographic Commission (IOC), the World Meteorological Organisation (WMO), the United Nations Environment Programme (UNEP), and the International Council of Scientific Unions (ICSU), during the period 1989–1993. Key milestones were the discussions on GOOS at the Second World Climate Conference in November 1990 and the United Nations Conference on the Environment and Development (UNCED). Many of the global objectives of GOOS were summarised in the oft-quoted Chapter 17 of the UNCED Conference Document "Agenda 21".

The development of GOOS requires political and diplomatic efforts involving all members of the UN family of nations and ICSU scientific councils. The overall governmental review of GOOS is provided by the Intergovernmental Committee (I-GOOS) and scientific guidance is provided by the Joint Scientific and Technical Committee (J-GOOS).

For more information please contact Nicholas Flemming:

ncf@unixa.nerc-wormley.ac.uk.

The Second WMO International Symposium on Assimilation of Observations in Meteorology and Oceanography

Robin Tokmakian, Department of Oceanography, Naval Postgraduate School, Monterey, CA 93943-5000, USA

This is a short note summarizing the international conference on assimilation held in Tokyo, Japan, 13-17 March 1995. The symposium was in two parts, of which the first was an intensive course on assimilation and the second part was a research conference. Publications are available for both parts of the symposium. The intensive course lecture notes are contained in a special volume of *The Geophysical Magazine, Series 2 (Vol. 1, 1995)* published by the Japan Meteorological Agency (Office of Archives and Library, Japan Meteorological Agency, 1-3-4 Otemachi, Chiyoda-ku, Tokyo 100, Japan, Fax: 81-3-3201-0682). The proceedings of the research conference are published by the World Meteorological Office (WMO/TD - No. 651, PWPR Report Series No. 5, Volumes I and II). The symposium attempted to cover both the disciplines of meteorology and oceanography equally, although there were more atmospheric scientists in attendance than oceanographers. This summary covers the areas relevant to oceanographers.

The intensive course began with lectures on what observations are available for assimilation from the atmosphere and the oceans (R. Atlas and A. Busalacchi). Emphasis was put on how the data sets differed on spatial and temporal scales and assimilation techniques can not be directly taken from atmospheric sciences to oceanography because of the sparseness of subsurface ocean data. The data from the TOGA, WOCE, and JGOFS programmes along with remotely sensed data from altimeters and infrared and visible sensors were mentioned as valuable data for ocean assimilations. The next two talks covered the models available for assimilation purposes for the atmosphere and the oceans (A. Arakawa and D. Anderson). Arakawa covered the basics of atmospheric modelling (types of models, grids, dynamical and physical adjustment mechanisms) of which some is valid for models of the ocean. D. Anderson emphasized the problems that are currently faced in ocean modelling: how to parameterize mixing, discretization of the vertical coordinate (levels vs. layers), topography, the accuracy of the forcing fields of momentum, heat and salt fluxes, and the use of free surface or rigid lid models.

The next three talks covered assimilation with O. Talagrand giving a general review of the subject (with an overview of the basic techniques: inverse theory, sequential and variational). A. Lorenc described the atmospheric side using the details of estimation theory to demonstrate what can be used to get a meaningful picture of atmospheric processes. P. Malanotte-Rizzoli reviewed oceanographic assimilation on a more general level, stating that the motivation for ocean assimilation is different than it is for the atmosphere. The objectives for ocean assimilation

are to make model improvements (improve parameterizations or correct model deficiencies), study dynamical processes, and to make ocean or climate forecasts. Examples of these objectives were given.

The specifics of assimilation techniques (variational: P. Courtier and sequential: M. Ghil) followed. Variational techniques include two, three and four dimensional data sets, univariate and multivariate. Examples were given from atmospheric uses. The Kalman filter was described using a simple one dimensional shallow water equation. Sequential methods work well for linear systems, but since the ocean and atmosphere have non-linear components, there is a need to develop nonlinear filters. Ghil suggested 2 methods: successive linearizations and 2nd-order moment truncation. The conclusion to Ghil's talk was that one can not have an observation system without data assimilation and one can not do assimilation without knowing the state of the model/data and the associated errors.

The last two lectures covered more specifics of assimilating data into models, one by N. Gustafsson on assimilating data into high resolution limited area models and P. de Mey's lecture on data assimilation at the resolution of the oceanic mesoscale. The first was generally an overview of the High Resolution Limited Area Modeling (HIRLAM) project among the Nordic countries, while the second covered methods that can be used in assimilating data into ocean models resolving the mesoscale. There is a problem that most mesoscale observations are from the ocean's surface and that something "special" has to be done to infer subsurface structure from the surface observations. De Mey mentioned that models and data need to be compared in a consistent statistical framework and more than any other ocean scale, the mesoscale is best described by statistics.

The last three days of the symposium involved an invited talk at the beginning of each session, followed by short talks of individual research efforts in a given area. The sessions were separated into the research directed toward specific techniques (sequential and variational) and the applications of these techniques in atmospheric and ocean research both on the large scale and on the mesoscale. For the ocean, presentations were given on assimilation of data into regional models (*e.g.* R. Miller, P. de Mey, J. Verron, M. Kamachi, I. Fukimori) and into global models, both large scale and mesoscale (*e.g.* H. Hurlburt, E. Tziperman, M. Bell).

On Wednesday evening, a panel discussion was held with the title "Data Assimilation for the Ocean and Atmosphere: What next?". The panel, chaired by E. Kalnay of NMC, consisted of D. Anderson (Oxford), A. Bennett (OSU), A. Busalacchi (NASA), P. Courtier (ECMWF),

N. Sato (JMA), and T. Schlatter (NOAA). For ocean modelling, there was a general agreement that the fluxes (momentum, heat and salt) are not good enough and more effort should be made to improve these fields before reasonable assimilations can be performed for realistic ocean studies. There needs to be improvement in coupled

ocean/atmosphere assimilations. There was also a discussion on the design of ocean observing systems, whether one time hydrographic lines or not. The main point was that the design (temporal and spatial) should consider how assimilation methods would incorporate the data into ocean models.

International WOCE Publications Since the Start of 1995

- | | | |
|--|---|--|
| <p>123/95 WOCE INTERNATIONAL PROJECT OFFICE 1995 Report of the twenty-first meeting of the WOCE Scientific Steering Group, WOCE-21, Institut für Meereskunde, Universität Kiel, Germany, 12–14 October 1994. 31pp.</p> <p>124/95 WOCE INTERNATIONAL PROJECT OFFICE 1995 Report of the seventh meeting of the WOCE Data Products Committee, DPC-7, James Rennell Centre for Ocean Circulation, Southampton, UK, 13–15 September 1994. 22pp.</p> <p>125/95 WOCE INTERNATIONAL PROJECT OFFICE 1995 Report of the ninth meeting of the WOCE Numerical Experimentation Group (NEG-9) and 1994 Workshop, Los Alamos National Laboratory, NM, USA, 19–21 September 1994. 24pp.</p> <p>126/95 WOCE INTERNATIONAL PROJECT OFFICE 1995 Overview of WOCE Activities: WHP-Moored Arrays – Floats – Drifters – XBTs – Sea Level – Satellites – Modelling – Data Information – Facilities. 56pp.</p> <p>127/95 WOCE HYDROGRAPHIC PROGRAMME</p> | <p>128/95 WOCE INTERNATIONAL PROJECT OFFICE 1995 Report of the thirteenth meeting of the WOCE Hydrographic Programme Planning Committee (WHP-13), College of Marine Sciences, National Sun Yat-Sen University, Kaohsiung, Taiwan, ROC, 2–4 November 1994. 23pp.</p> <p>129/95 WOCE INTERNATIONAL PROJECT OFFICE 1995 Report of the seventh meeting of the WOCE/TOGA Surface Velocity Programme Planning Committee (SVP-7), Sea Lodge at La Jolla Shores, CA, USA, 2–4 November 1994. 31pp.</p> <p>130/95 WOCE INTERNATIONAL PROJECT OFFICE 1995 The status, achievements and prospects for WOCE (1995): the background to the World Ocean Circulation Experiment; its present status and achievements; a strategy for the future. 30pp.</p> | <p>SPECIAL ANALYSIS CENTRE 1995 Gouretski, V., and K. Jancke. A consistent pre-WOCE hydrographic data set for the South Atlantic: Station data and gridded fields. WHP SAC Technical Report No. 1. 80pp.</p> |
|--|---|--|

Note on Copyright

Permission to use any scientific material (text as well as figures) published in the International WOCE Newsletter should be obtained from the authors.

WOCE is a component of the World Climate Research Programme (WCRP), which was established by WMO and ICSU, and is carried out in association with IOC and SCOR. The scientific planning and development of WOCE is under the guidance of the JSC Scientific Steering Group for WOCE, assisted by the WOCE International Project Office. JSC is the main body of WMO-ICSU-IOC, formulating overall WCRP scientific concepts.

The WOCE Newsletter is edited at the WOCE IPO at the Institute of Oceanographic Sciences Deacon Laboratory, Brook Road, Wormley, Godalming, Surrey, GU8 5UB, UK (Tel: 44-1428-684141, Fax: 44-1428-683066, email: woceipo@unixa.nerc-wormley.ac.uk). Financial support is provided by the Natural Environment Research Council, UK.

We hope that colleagues will see this Newsletter as a means of reporting work in progress related to the Goals of WOCE as described in the Scientific Plan. The SSG will use it also to report progress of working groups, experiment design and models.

The editor will be pleased to send copies of the Newsletter to institutes and research scientists with an interest in WOCE or related research.

Meeting Timetable 1995

WOCE Meetings

September 12–15	US WOCE SSC	Seattle
October 3–5	US WOCE Synthesis Meeting	Irvine, CA
October 10–12	WHPPC-14	Hamburg
mid-October	(C)WXXPPC-4	Ottawa
October 26–27	SMWG-1	Boston
October 31–November 3	WOCE-22	WHOI

Science and other Meetings

June 26–29	The Seas of Southeast Asia – the Key to Regional Climate Patterns, Lombok
July 2–14	IUGG XXI General Assembly, Boulder
August 5–12	IAPSO XXI General Assembly, Honolulu
September 4–8	3rd International Conference on Modelling of Global Climate Change and Variability, Hamburg
September 21–29	ICES 1995 Annual Science Conference, Copenhagen
September 26–29	42nd Annual Eastern Pacific Oceanic Conference (EPOC) (special topic: Eastern Boundary Currents), Fallen Leaf Lake, California
September 25–29	IGBP – Global Analysis Interpretation and Modelling, Garmisch
October 10–14	5th International Conference on Paleoceanography, Halifax
October 16–20	Tracer workshop (Ewing Symposium), Lamont or Arizona
October 16–20	Operational Oceanography and Satellite Observation, Biarritz
October 16–22	4th Annual Meeting of the North Pacific Marine Science Organisation (PICES) (with a session on circulation in the subarctic North Pacific and its marginal seas), Qingdao
October 24–27	WCRP Workshop on Air-Sea Flux Fields for Forcing Ocean Models and Validating GCM's, Reading, UK

For more information on the above meetings contact the IPO. If you are aware of any conferences or workshops which are suitable for the presentation of WOCE results and are not mentioned in the above list please let the IPO know.

WOCE Workshops

In October 1994 the WOCE SSG approved an outline strategy for the presentation and publication of WOCE results. This strategy includes science workshops at which results from a particular ocean basin will be presented and intercompared.

The possible timetable, based on present estimates of the data flow, is:

Pacific Ocean	1996
Southern Ocean	1997 (Australia)
Indian Ocean	1998
North Atlantic	1999

Except for the Southern Ocean workshop we are still looking for countries/organisations who would like to host and support the above WOCE workshops.

Please contact the WOCE IPO for more information.